Exon, N.F., Kennett, J.P., Malone, M.J., et al., 2001
Proceedings of the Ocean Drilling Program, Initial Reports Volume 189

4. SITE 1169[1]

Shipboard Scientific Party[2]

PRINCIPAL RESULTS

Site 1169 is located in deep water (3568 m) in a flat plain on the western part of the South Tasman Rise (STR), 400 km south of Tasmania. It lies 30 km east of the ridge of the Tasman Fracture Zone (TFZ) that rises 400 m above the plain. The site is ~100 km south of the Subtropical Front (Subtropical Convergence). At Site 1169 we planned to penetrate open-ocean carbonate oozes deposited from the Miocene onward as Australia moved northward from Antarctica. In the early Miocene (20 Ma), the site was at 55°S compared to its present latitude of 47°S. The primary objective was to core a complete upper Neogene sequence with high sedimentation rates in northern subantarctic waters for high-resolution biostratigraphic and paleoclimate investigations.

Seismic profiles indicate that the site is in a westerly thickening wedge of transparent young Neogene ooze, ~200 m thick at the site, that apparently onlaps a prominent reflector and unconformity, below which is more transparent ooze or chalk. This wedge of ooze appears to have been deposited in the lee of the western ridge (TFZ), which provided protection from scouring by the easterly flowing Antarctic Circumpolar Current. The results from Site 1170, where a comparable section was drilled in shallower water to the east, show that the transparent wedge results from facies change rather than younging westward.

We had planned to core three advanced hydraulic piston corer/extended core barrel (APC/XCB) holes, but poor weather conditions and large heaves greatly degraded the quality of the cores, and only Hole 1169A was cored to 246.3 mbsf with 91.4% recovery (Table T2, p. 94, in the "Leg 189 Summary" chapter). Although recovery was high in the APC cores, flow-in and other disturbances meant that both core structure and age reliability were severely compromised. This will preclude future high-resolution paleoclimatic investigations.

---

[1] **Examples of how to reference the whole or part of this volume.**
[2] **Shipboard Scientific Party addresses.**

Ms 189IR-104

The drilled sequence consists of 246.3 m of nannofossil ooze with a total age range from the late Miocene (12.2 Ma) to the late Quaternary, although two disconformities removed much of the record. The upper ~200 mbsf of the sequence represents the last ~4 m.y. and disconformably overlies a thin (~200 to 220 mbsf) sequence of late Miocene age (6.5 to 6.8 Ma). This, in turn, is underlain by sediments of middle Miocene age (~12.5 Ma), although strong sediment disturbance makes for difficult dating in this part of the sequence. This time break is correlated with a seismic unconformity. Sediments are dominated throughout by nannofossil ooze with rare to common foraminifers and siliceous microfossils that include diatoms and radiolarians. Siliciclastic sediment components are largely absent in this open-ocean location. One lithostratigraphic unit is recognized, which is subdivided into two subunits: Subunit IA (0–170.1 mbsf) is a nannofossil ooze with common to abundant siliceous microfossils; Subunit IIB (170.1–246.3 mbsf) is a nannofossil ooze with rare to few siliceous microfossils. Sedimentation rates were low (1.6 cm/k.y.) during the Quaternary through late Pliocene, very high (20 cm/k.y.) during the early Pliocene, and moderately high (10.9 cm/k.y.) during the brief late Miocene interval represented. The nannofossil oozes were deposited in upper abyssal water depths under well-oxygenated bottom-water conditions.

Although the primary objective, high-resolution climatic history, could not be met, Site 1169 provides a number of highlights. We were able to develop a useful, although relatively broad, integrated subantarctic biostratigraphy for the Pliocene and Quaternary involving planktonic foraminifers, calcareous nannofossils, diatoms, radiolarians, and organic dinocysts. Ostracodes are also persistently present throughout. Few previous sites from the subantarctic region have allowed the development of such an integrated stratigraphy, particularly from the Australian sector of the Southern Ocean. This site also contains the southernmost late Neogene dinocyst record ever found. A conspicuous level of microtektites was discovered in association with the latest Miocene/earliest Pliocene disconformity, the first of this age to be reported from the Southern Ocean. Conspicuous late Miocene unconformities suggest intensification of bottom-water circulation during that time and associated carbonate dissolution on the STR at depths close to 3.5 km.

Planktonic microfossil assemblages reflect the influence of both subantarctic and temperate water masses in this northern subantarctic location. These mixed assemblages may indicate shifts in position of the Subtropical Convergence over the region. Antarctic elements are also present in some planktonic microfossil groups, reflecting influence of more highly productive antarctic surface waters to the south. The very high sedimentation rates of the early Pliocene at this site have previously been observed over broad areas of the South Pacific and elsewhere (Kennett, von der Borch, et al., 1986). These high rates were considered to represent a significant increase in calcareous biogenic productivity associated with fundamental paleoceanographic changes affecting surface waters during early Pliocene warmth. Rates of early Pliocene biogenic sedimentation at Site 1169 may have been further amplified by winnowing of calcareous nannofossils from the STR into the local catchment basin in which Site 1169 is located. Site 1169 extends observations for the first time to the subantarctic region of remarkably high early Pliocene biogenic productivity.

BACKGROUND AND OBJECTIVES

Site 1169 is located in present-day upper abyssal water depths (~3570 m) on the western part of the STR near its western margin at ~47°S in northern subantarctic waters (Fig. F3, p. 68, in the "Leg 189 Summary" chapter). The site is located in thick, almost flat-lying sediments accumulated in a shallow basin on a gentle structural low formed on the Cretaceous surface (Exon et al., 1997). The younger part of the Neogene section is seismically transparent and has accumulated in the lee of the Tasman Fracture Zone, which forms a ridge to the west. The older Neogene section is well bedded but hummocky in character and probably consists of chalks with some hiatuses. The lowest part of the Neogene may be absent. The seismically similar underlying Eocene sequence is probably largely mudstone.

Site 1169 was selected at the intersection of multichannel seismic profiles *Tasmante* 125-4 (Fig. F1) and -9. This shallow-penetration site was designed to fully recover a thick, young Neogene sequence. We planned to penetrate 0.23 s (195 m) of Pliocene to Holocene transparent ooze that apparently onlapped 0.22 s (185 m) of upper Oligocene to Miocene ooze and chalk above an inferred Oligocene unconformity. Below the Oligocene unconformity is 0.1 s (110 m) of presumed upper Eocene to lower Oligocene marine mudstone, marl, and chalk, above 0.08 s (90 m) of presumed middle Eocene mudstone. The base of the site at 246.3 mbsf was shown to be middle Miocene, and the upper onlapped surface was just ~30 m above the base.

F1. A portion of seismic line *Tasmante* 125-04 through Site 1169, p. 27.

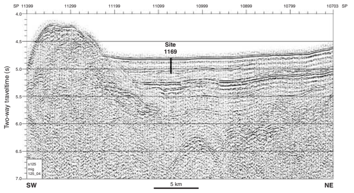

The primary objective of Site 1169 was to core a complete late Neogene sequence of high sedimentation rate in northern subantarctic waters for high-resolution biostratigraphic and paleoclimatic studies. The depths are sufficiently shallow to provide a high-quality carbonate biogenic sequence and at a high enough latitude for preservation of both calcareous and siliceous microfossils as proxies for paleoclimatic change. This location was specifically selected because of seismic stratigraphic data indicating a sequence of especially high sedimentation rate that would allow high-resolution paleoclimatic investigations. Site 1169 would also provide basic biostratigraphic records for several microfossil groups of late Neogene age from the northern subantarctic of the Pacific/Indian Ocean region. These would complement such records obtained from the subantarctic region south of South Africa (Shipboard Scientific Party, 1999).

To the north of Site 1169 is the Subtropical Front (Subtropical Convergence), which marks the northern limit of subantarctic surface waters and the Southern Ocean and is marked by a strong surface-water temperature gradient of ~4°C (from 14° to 18°C in summer) and a temperature of 11°C at 150 m (Tchernia, 1980; Rintoul et al., 1997; Sikes 1995). Site 1169 lies north of the Subantarctic Front marked by a surface-water temperature gradient of 6°–8°C (Rintoul et al., 1997). This forms the boundary between the Australasian surface water and Circumpolar Subantarctic surface water (Heath, 1985). Subantarctic waters are driven to the east by often strong prevailing westerlies as part of the Circumpolar Current. The subantarctic water mass is bounded to the south by the Antarctic Polar Front or Convergence, a major boundary marked by the 2°C vertical isotherm in winter (Barrows et al., 2000) and considered the northern limit of the antarctic zone.

Site 1169 is well located to have recorded meridional movement of surface-water masses including the oceanic fronts separating major water masses (Sikes, 1995). Today, the Subtropical Convergence overlies the STR, and the Polar Front is only a few degrees to the south. At 3500 m, Site 1169 lies within Circumpolar Deep Water and has the potential to record changes in this water mass that may be linked with oscillations in the strength of the so-called oceanic conveyor belt circulation.

The Southern Ocean is considered to be very important in Quaternary global climate change as it certainly was earlier in the Cenozoic. Very high biological productivity of the Southern Ocean in combination with major regional production of deep and intermediate waters strongly influence atmospheric CO_2 levels and, hence, global climate (Broecker et al., 1980; Mortlock et al., 1991; Howard and Prell, 1992). Quaternary climatic changes in the Southern Ocean have been large and on Milankovitch scales, as documented by changes in the extent of sea ice, sea-surface temperatures, water-mass boundaries, deep- and intermediate-water production, and biological productivity of surface waters. The relative importance of North Atlantic and Southern Ocean sources of deep waters to the ocean has oscillated during the late Quaternary with major implications for climate change (Boyle and Keigwin, 1985; Charles et al., 1996). The subantarctic region is a repository of paleoclimatic information critical for better understanding of late Neogene climatic processes and variability. Site 1169 was designed to obtain records for such investigations.

OPERATIONS

Transit to Site 1169 Via Hobart

The transit from Site 1168 to the Port Huon pilot station for a personnel transfer was accomplished at an average speed of 12.6 kt, which put the vessel at the mouth of the D'Entrecasteaux Channel at 0900 hr, >4 hr ahead of schedule. After reviewing the option of remaining stationary and waiting for the pilot boat to transit to the vessel, we decided to continue directly to the innerpilot station near Hobart, arriving at 1245 hr on 28 March.

The ship rendezvoused with the pilot boat, and three new personnel (two from the Ocean Drilling Program [ODP] and one from Overseas Drilling Limited) were transferred on board along with some light cargo. Two personnel, an ODP engineer and a technical representative from Maritime Hydraulics, left the vessel. At 1255 hr, the transfer was completed and the *JOIDES Resolution* altered course and continued to the next site. The vessel proceeded on a southerly course for the 270-nmi transit, which was accomplished at an average speed of 11.3 kt.

Hole 1169A

At 1245 hr on March 28, a beacon was deployed, hydrophones and thrusters were extended, and the vessel settled on location. An APC/XCB bottom-hole assembly (BHA) was made up and run to near the precision depth recorder depth of 3584.4 mbrf.

As the drill string was being deployed, a cold front passed over our location, driving the winds from 28 kt to >55 kt in the space of a few minutes. Accompanying the arrival of the front were very heavy rains and a drop in temperature of 4°C in <15 min. Although the intensity of the winds quickly abated as the direction shifted from the north to the west, the resulting conditions from the passage of the front strongly affected subsequent coring.

Hole 1169A was spudded with the APC at 2245 hr on 28 March. The seafloor depth was calculated from the recovery of the first core and determined to be 3578.9 mbrf, or 3567.9 mbsl. As piston coring was initiated, the weather deteriorated and generated considerable vessel motion that adversely affected the quality of the cores. During coring in this hole, the winds were predominantly from the west and never dropped below 22 kt with gusts frequently measured between 35 and 40 kt. There was also a complex swell from the west and southwest (~5 m amplitude) that would periodically combine and push the vessel heave >6 m.

The weather made for difficult operations with resulting poor quality of the piston cores. During operations, the wireline had to be re-terminated at the rope socket twice because of fraying steel-rope members arising from an excessive bending radius caused by excessive vessel motion. Two additional wireline round-trips were needed to fish out the core barrel when the wireline eventually parted at the rope socket. On another occasion, coring had to be stopped for several hours while the drill crew disassembled the piston corer to clean out a core liner that completely failed, likely a result of the extreme hydraulic forces. The wireline speed was also reduced to accommodate the weather-induced motion of the drill string and vessel.

The quality of the cores was poor because of the flow-in and vertical disturbance caused by the dynamics of attempting to piston core in this environment. During piston coring, the heave compensator is not used except for drilling or washing ahead to position the drill bit for the next piston core attempt. When the piston corer is fired, the heave compensator is locked and the bit is forced to follow the vertical motion of the vessel. It was expected that as soon as XCB coring was initiated, the core quality would improve because of the activation of the heave compensator with a resulting decrease in core disturbance. Unfortunately, the main objective for this site was recovery of an upper Neogene section for high-resolution analysis that only undisturbed APC cores could provide.

After the APC coring advanced to a depth of 199 mbsf, we switched to the XCB system in an attempt to minimize core disturbance, despite the fact that only minimum pull-out force was required to free the core barrel from the sediment. Coring concluded when the XCB deepened the hole from 199 mbsf to the depth objective of 247 mbsf. The main goal for this site was high-resolution analysis of the sedimentary record; hence, operations were terminated because of the effect that the sea state was having on core quality. The average recovery of the piston-cored section of the hole was 100%, with overall recovery being 91% (Table T1).

T1. Coring summary, p. 48.

The drill bit was pulled clear of the seafloor at 0200 hr on 31 March, and the drill string was recovered. As the BHA was being disassembled into the component drill collars in preparation for the transit to the next site, the beacon was successfully recovered. Following the retraction of the thrusters and hydrophones and the securing of the drilling equipment, the vessel began the short transit to the next site at 0830 hr on 31 March.

LITHOSTRATIGRAPHY

Introduction

At Site 1169, one hole with 26 cores was drilled. Hole 1169A reached 246.3 mbsf with a total sediment recovery of 91.4% using the APC and XCB (Fig. F2). The sediments at Site 1169 mainly consist of pelagic nannofossil ooze with minor constituents such as foraminifers and siliceous microfossils. Siliciclastic components were rarely observed. Because the entire sediment sequence at the site exhibits no major lithologic changes, only one unit is recognized. Unit I, with two subunits differentiated, shows relatively minor differences in core features, smear slides, reflectance spectrophotometry, and coulometric carbonate analyses. Two hiatuses were recognized, at ~220 and ~200 mbsf, based on multitaxa biostratigraphy.

F2. Lithostratigraphic summary, p. 28.

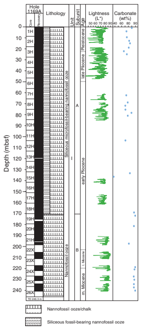

The primary site objective was to obtain late Neogene high-resolution (i.e., Milankovitch scale) paleoceanographic data in the subantarctic. Although the overall recovery was relatively high, the piston-cored sediments (Cores 189-1169A-1H through 21H) were moderately to strongly disturbed during the drilling operation, whereas no significant drilling disturbance occurred for XCB drilled cores below Core 189-1169A-22X (Fig. F2). The coring disturbances for APC sediments resulted from heavy swell, strong winds, and related technical problems such as crushed and split liners. No further attempt was made to drill the scheduled B and C holes at this site because of the severe weather conditions. The relative intensity of sediment disturbance is shown in Figure F3A. Severely disturbed soupy (e.g., Cores 189-1169A-1H, 2H, and 11H) and vertically deformed (e.g., Cores 189-1169A-4H, 5H, 10H, and 15H) sediments hampered our measurements of several chemical and physical properties. Although high-resolution data could not be collected from the disturbed sediments, measurements of several sedimentary parameters exhibit trends that have aided interpretations of general changes in depositional environments.

F3. Physical and chemical properties, p. 29.

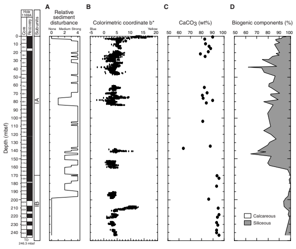

Description of Lithostratigraphic Units

Unit I

Depth: 0 to 246.3 mbsf
Age: Pleistocene to middle Miocene
Interval: Cores 189-1169A-1H through 26X
Thickness: 246.3 mbsf

Unit I consists of 246.3 m of middle Miocene to Pleistocene pelagic nannofossil ooze with rare to common foraminifers and siliceous fossils including radiolarians, diatoms, silicoflagellates, and sponge spicules. The sediments of Unit I are generally massive and exhibit no notable sedimentary structures, except for sporadic occurrences of isolated light bluish gray thin to medium laminations and small (~10 mm) in situ black pyrite concentrates. Occasionally, dark pyritic thin beds were observed (e.g., Core 189-1169A-17H). The color of sediments varies from light greenish gray to white. Calcium carbonate content is relatively high throughout the unit, ranging between 78.9 and 95.5 wt%, except for an anomalous low value of 63.8 wt% measured at 137.32 mbsf (Sample 189-1169A-15H-4, 72 cm) (see "Organic Geochemistry," p. 19). The APC-cored sediments (i.e., Cores 189-1169A-1H through 21H) show a variety of coring disturbance features in many intervals (Fig. F3A) that prevented us from observing detailed sedimentary structures. No coring disturbance was observed for the XCB-drilled cores below Core 189-1169A-22X.

In spite of the above-mentioned drilling disturbances, two subunits have been recognized within Unit I at Site 1169. Subunit IA (0–170.1 mbsf) is characterized by light greenish gray to light gray nannofossil ooze with common to abundant siliceous microfossils, mostly diatoms, sponge spicules, and bioclasts, as modifiers. The average calcium carbonate content for the Subunit IA sediments is 84.4 wt%. The difference between Subunits IA and IB is the minor biogenic components—Subunit IB (170.1–246.3 mbsf) is purely composed of nannofossil ooze. The representative lithologic color of Subunit IB is white. Its calcium carbonate content averages 93.5 wt%, higher than that of Subunit IA.

The boundary between Subunits IA and IB is placed between Cores 189-1169A-18H and 19H, based on changes in sediment color and percent content of siliceous fossils. The siliceous fossil-bearing greenish gray nannofossil ooze of Subunit IA changes to white pure nannofossil ooze of Subunit IB at the bottom of Core 189-1169A-18H. Although disturbed during coring, the sediments in Cores 189-1169A-17H and 18H are transitional in color and siliceous fossil content from Subunits IA to IB facies (Fig. F3). Biostratigraphic studies at this site suggest the presence of a major hiatus between Samples 189-1169A-23X-CC and 24X-CC (~218 mbsf), possibly spanning much of the middle Miocene to late Miocene, and a lesser one between Samples 189-1169A-21H-CC and 22X-CC (~200 mbsf), removing part the late Miocene to early Pliocene (see **"Biostratigraphy,"** p. 9).

Subunit IA

Depth: 0 to 170.1 mbsf
Age: Pleistocene to early Pliocene
Interval: Cores 189-1169A-1H through 18H
Thickness: 170.1 mbsf

Subunit IA consists predominantly of light greenish gray to light gray (10GY 8/1 to N 7) siliceous fossil-bearing nannofossil ooze. Throughout the subunit, siliceous fossils such as diatoms, sponge spicules, silicoflagellates, and radiolarians are present. The percent estimates of the biogenic components examined under smear slides, as plotted in Figure F3D, exhibit a sharp decrease in siliceous contents between 160 and 170 mbsf, where the subunit boundary is placed. The calcium carbonate content of Subunit IA sediments averages 84.4 wt%, ranging between 78.9 and 89.9 wt% (Fig. F3C). Minor amounts of foraminifers, calcareous bioclasts (fragments of biogenic materials such as foraminifers and ostracodes), and clay are found in the nannofossil ooze throughout the subunit. Nannofossil oozes in the upper part (Cores 189-1169A-1H through 3H) of the subunit contain noticeable amounts of foraminifers and bioclasts. These foraminifer- and bioclast-bearing nannofossil oozes are very pale brown (10YR 8/3 to 7/3), reflecting more abundant calcareous fossils (Fig. F3D).

Subunit IB

Depth: 170.1 to 246.3 mbsf
Age: early Pliocene to middle Miocene

Interval: Cores 189-1169A-19H through 26X
Thickness: 76.2 mbsf

Subunit IB consists mainly of uniform white (N 8), pure nannofossil ooze. Occasionally, minor changes to light greenish gray (10GY 8/1) were observed. The calcium carbonate content of the subunit is generally higher compared with Subunit IA, ranging between 93.3 and 95.5 wt%, with an average value of 93.5 wt%. Contents of siliceous fossils are extremely low (Fig. **F3D**). Spectrophotometry lightness (L*) measurements exhibit a slight increase across the Subunit IA/IB boundary (Fig. **F2**).

Although not apparent in calcium carbonate content or spectrophotometry lightness (L*) measurements, an interval of light yellowish white (2.5Y 8/2) nannofossil ooze is observed between 208 and 211 mbsf in Core 189-1169A-23X. This visual color feature is also recognized by the spectrophotometry (b*) signals (Fig. **F3B**). In Sample 189-1169A-22X-CC, of early Pliocene age, spherical microtektites were found.

Interpretations

Despite drilling disturbances in the Site 1169 APC cored sediments, various proxies captured long-term trends in the Neogene climatic evolution at the site. The major hiatus (or severely condensed section) recognized between Sections 1169A-23X-CC and 24X-CC, ranging from the middle Miocene (tentatively, ~12.5 Ma) to late Miocene (~6.9 Ma), implies strong deep-water circulation and resulting submarine erosion and/or dissolution of calcium carbonate at the site. It corresponds to an unconformity in seismic profiles (see **"Background and Objectives,"** p. 3). This hiatus may be associated with the development of vigorous bottom-water circulation in the Southern Ocean that is inferred to have developed with the middle Miocene expansion of the East Antarctic Ice Sheet that started at ~14 Ma (Woodruff and Savin, 1989; Flower and Kennett, 1995). However, no microfossil datum was found below the hiatus, leaving the timing of its onset at Site 1169 unclear.

The light yellowish white nannofossil ooze observed between 208 and 211 mbsf in Core 189-1169A-23X, which encompasses or overlies the hiatus (condensed section), may reflect an incursion of oxygenated, relatively "young" water to the seafloor, supporting the hypothesis that the production of antarctic deep water intensified during the middle Miocene. Because the middle to late Miocene hiatus was not found at the shallower water depth at Site 1168, the circulation of the cold bottom water apparently affected deeper water depths only, at least between 12.5 and 6.9 Ma.

The early Pliocene pelagic sediments recovered at Site 1169 are unusually thick. Between 60 and 200 mbsf (~4.6–4.0 Ma), the linear sedimentation rate is 23.4 cm/k.y. This sedimentation rate is the highest recorded from the Southern Ocean. The transition from pure nannofossil ooze (Subunit IB) to diatom-bearing nannofossil ooze (Subunit IA) occurred at ~4.5 Ma, nearly coinciding with the onset of a high-sedimentation-rate period. Despite this increase in silica content, the majority of sediment in Subunit IA is composed of nannofossils (>84%) (Fig. **F3D**).

The factors that controlled this early Pliocene high-sedimentation rate are of particular interest. Because the material accumulated during this interval is mostly pelagic biogenic in origin (i.e., nannofossils and diatoms), the possibility of dilution by a nonbiogenic component is excluded. The other possible factors are increase in productivity, redeposition of winnowed materials, or a combination of both. Incursion of nutrient-rich waters to the site, probably associated with southward migration of the Subtropical Front and/or regional upwelling, may have stimulated nannoplankton productivity and induced an enormous flux of carbonate in the region. Such high-primary productivity may be responsible for the increase in siliceous fossil content at the site. Redeposition of reworked or winnowed materials may also have contributed to the elevated sedimentation rate at Site 1169.

The episode of early Pliocene amplified sedimentation rate is also documented from other areas in the Pacific Ocean. Specifically, the magnitude of the early Pliocene sedimentation rate increase in the Tasman Sea (Deep Sea Drilling Project [DSDP] Sites 590 through 594) is comparable to that of Site 1169. Nelson (1986) attributed the elevated Pliocene sedimentation rate observed in the Tasman Sea to increased calcareous biogenic productivity. Although it appears that increase in biogenic productivity is responsible for the early Pliocene high sedimentation rate, the causes of concurrent occurrence of the event in various locations remain unclear.

BIOSTRATIGRAPHY

Site 1169 is situated beneath present-day subantarctic waters on the western part of the STR (Hole 1169A is located at latitude 47°03.9159′S) in upper abyssal water depths (3568 m). A high degree of sediment flow and disturbance was encountered within the recovered cores for Hole 1169A. Soft-sediment deformation and downhole caving complicated the biostratigraphy, therefore only last occurrence (LO) events are used in the final age model (Fig. **F4**). Seven major microfossil groups recovered from core-catcher samples are used to constrain the base of Hole 1169A to no older than 13.6 Ma (middle Miocene) and to construct an age-depth model. The youngest core (189-1169A-1H) is assigned to the middle Pleistocene on biostratigraphic and paleomagnetic information (see also **"Paleomagnetism,"** p. 17). The biostratigraphic data suggest the presence of two hiatuses; the younger spans the Miocene/Pliocene boundary and the older straddles the middle Miocene/upper Miocene boundary. Reconstructed linear sedimentation rates imply enhanced calcareous nannofossil production during the early Pliocene, demonstrated for the first time in the subantarctic. In addition, Hole 1169A contains the most southerly late Neogene dinoflagellate cyst (dinocyst) record discovered to date. There are few subantarctic sites where such a broad range of microfossil groups are present, affording a unique opportunity for a highly integrated multiple-group biostratigraphy.

F4. Site 1169 age-depth plot and linear sedimentation rates, p. 31.

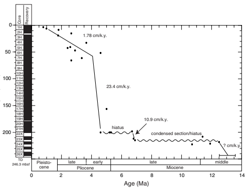

Fluctuations in the abundance of cold- and warm-water dinocysts and siliceous microfossils (diatoms and radiolarians) in the Pliocene–Pleistocene signify possible meridional shifts in the position of the Subtropical Convergence during this time. Deposition at abyssal paleodepths throughout the sequence is inferred from the benthic foraminifers.

Calcareous Nannofossils

All core-catcher samples as well as additional samples from some critical intervals were examined for calcareous nannofossils at Site 1169.

Calcareous nannofossils are generally abundant and well to moderately preserved throughout the cored interval (Table T2). Poor coring conditions at this site resulted in Cores 189-1169A-1H through 21H being highly disturbed and Cores 189-1169A-22X through 26X having low recovery (see **"Lithostratigraphy,"** p. 6). The nannofossil biostratigraphy (Table T3) for the middle Miocene through the Pleistocene sediments should be considered with these limitations in mind.

T2. Distribution and abundance of nannofossils, p. 49.

T3. Calcareous nannofossil datum levels and their assigned age estimates, p. 50.

Sample 189-1169A-1H-CC contains *Pseudoemiliania lacunosa* but not *Emiliania huxleyi*. Toothpick samples were taken through Core 189-1169A-1H in an effort to establish the first occurrence (FO) of *Emiliania huxleyi* (0.26 Ma) and the LO of *P. lacunosa* (0.45 Ma). Analysis of these samples revealed successive events taking place in a haphazard order indicating core disturbance or strong bioturbation. The FO of *E. huxleyi* and the LO of *P. lacunosa* could not be located within Core 189-1169A-1H to any degree of confidence.

The LO of *Discoaster brouweri* (1.95 Ma) and the LO of *Discoaster surculus* (2.55 Ma) are found between Samples 189-1169A-2H-CC and 3H-CC (Table T3). Toothpick samples taken from Core 189-1169A-2H showed similar disturbance to Core 1H, and these datums could not be separated. The Pliocene/Pleistocene boundary, which is marked by the LO of *D. brouweri* in low latitudes or approximated by the LO of *Calcidiscus macintyrei* (1.67 Ma) in nontropical areas where discoasters are rare, is therefore placed between Samples 189-1169A-1H-CC and 2H-CC based on the latter datum.

The LO of *Reticulofenestra pseudoumbilicus* (3.75 Ma) is found between Samples 189-1169A-3H-CC and 4H-CC, marking the lower Pliocene/upper Pliocene boundary. The base of nannofossil Zone CN11 at 4.6 Ma is marked by the LO of *Amaurolithus primus* between Samples 189-1169A-4H-CC and 5H-CC. *Ceratolithus acutus* and *Discoaster quinqueramus* are not encountered, and the Miocene/Pliocene boundary can not be identified by nannofossil biostratigraphy.

Samples 189-1169A-7H-CC through 22X-CC yield abundant, well-preserved nannofossil assemblages that do not provide useful age information. These assemblages are dominated by *Calcidiscus leptoporus, C. macintyrei,* and *Coccolithus pelagicus* with a few reticulofenestrids.

The base of the late Miocene calcareous nannofossil Subzone CN9b is placed between Samples 189-1169A-23X-3, 44 cm, and 23X-4, 25 cm, based on the LO of *Discoaster loeblichii* (6.8 Ma). The LO of *Amaurolithus delicatus* is recorded between Samples 189-1169A-23X-CC and 24X-1, 120 cm. Although this species is rare in Hole 1169A, its LO at 6.9 Ma in this interval is in good agreement with bioevents above and below this interval. The FO of *D. loeblichii* (8.7 Ma) between Samples 189-1169A-24X-1, 120 cm, and 24X-2, 60 cm, may have been shifted downhole in this disturbed section by caving or other means, and this datum has not been included in the construction of the age-depth model for this site (see **"Age Model and Sedimentation Rates,"** p. 16). The LO of *Cyclicargolithus floridanus* (11.9 Ma) is present between Samples 189-1169A-24X-3, 10 cm, and 24X-4, 35 cm. This datum generally lies below the upper Miocene/lower Miocene boundary (Gartner, 1992).

The last three datums are present within 7.9 m and span 5.0 m.y. This indicates a condensed section or hiatus between Sample 189-1169A-23X-CC and 24X-4, 35 cm. The break in sedimentation appears to be between Sample 189-1169A-23X-CC and 24X-1, 120 cm, indicated by 120 cm of sediment representing 1.8 m.y. (0.07 cm/k.y. sedimentation rate). An even less optimistic interpretation of the nannofossil data, ignoring the FO of *D. loeblichii* as possibly being reworked and using the LO of *C. floridanus* at 11.9 Ma, would result in 5.0 m.y. being represented by 6.4 m of sediment (0.12 cm/k.y. sedimentation rate).

A distinct color change (Fig. **F5**) is observed in Core 189-1169A-23X (see **"Lithostratigraphy,"** p. 6). The nannofossil ooze gradually changes from white (N8) to light greenish gray (5GY 8/1) in Section 189-1169A-23X-3, and a change in color reflectance data trends is seen at Sample 169-1169A-23X-3, 124 cm. Analysis of toothpick samples from this core suggests a change in paleowater temperatures across this interval. The overlying white nannofossil ooze is interpreted as representing cooler waters as indicated by the lack of discoasters in addition to the low diversity and high abundance of placoliths. The light greenish gray nannofossil ooze is interpreted to represent warm-water conditions based on the sudden influx of numerous, well-preserved specimens of discoasters. The LO of *D. loeblichii* between Samples 189-1169A-23X-3, 44 cm, and 23X-4, 25 cm, at 6.8 Ma provides good age control for this event. The LO of the diatom *Actinocyclus fryxellae* (6.7 Ma) between Sections 189-1169A-20H-CC and 21H-CC indicates that this water-mass change was not accompanied by a recorded hiatus in sedimentation.

F5. Color changes associated with water temperature shift, p. 32.

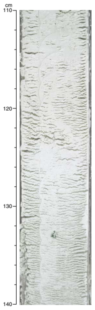

Analysis of abundant Neogene nannofossils from Site 1169 indicates a well-preserved "mixed" assemblage. Despite the subantarctic location of Site 1169 neither warm-water nor cold-water assemblages dominate the record. At least one hiatus or condensed section is indicated by the nannofossil biostratigraphy. Further study of Cores 189-1169A-7H through 22X may yield additional biostratigraphic datums, but the quality of the cores recovered at Site 1169 may preclude higher resolution results.

Planktonic Foraminifers

In general, the planktonic foraminiferal assemblages (>250 µm) are temperate in composition, dominated by species belonging to the *Globoconella* plexus. Other species common throughout the section are *Globigerina bulloides, Globigerina falconensis, Globigerina quinqueloba, Neogloboquadrina pachyderma, Orbulina universa, Globorotalia crassaformis,* and *Globigerinita glutinata* (see Table **T4**). Though the diversity of the assemblages is low, the populations are large. Characteristics of the populations of the various species seem to change with time and are probably related to the changing environmental conditions associated with movements in the Subtropical and Subantarctic Fronts. Future isotopic studies may provide an insight into these faunal variations. The zonal scheme as discussed in **"Biostratigraphy,"** p. 9, in the "Explanatory Notes" chapter seems to be readily applied to these assemblages. The distribution of species in these samples is given in Table **T4.**

T4. Range chart of planktonic foraminifers, p. 51.

Quaternary (Pleistocene/Holocene)

Samples 189-1169A-1H-CC and 2H-CC both contain *Globorotalia truncatulinoides,* indicating Zone SN14. Thus, the *G. truncatulinoides* FO (1.96 Ma) is restricted to the interval between 15.04 and 27.90 mbsf. Planktonic foraminifers are abundant and well preserved.

Pliocene

The uppermost planktonic foraminifer zone of the Pliocene (*Globorotalia inflata* Zone; SN13) was not recognized in Hole 1169A. Therefore, the *G. inflata* Zone is either present within a highly condensed interval between 15.04 and 27.90 mbsf or absent altogether. Samples 189-1169A-3H-CC through 6H-CC contain *Globorotalia puncticulata* without either *G. inflata* or *Globorotalia pliozea,* indicative of Subzone SN12b. This subzone, the *G. puncticulata* Subzone, is highly expanded in Hole 1169A, spanning the interval bounded by Samples 189-1169A-3H-CC and 21H-CC, roughly 130 m of section. Between Sections 189-1169A-7H-CC and 21H-CC, samples contain a typical Subzone SN12b assemblage, but many specimens of *G. inflata* are present in most of the assemblages, indicating contamination from above. In general, planktonic foraminifers are abundant and well preserved throughout this interval.

Sample 189-1169A-22X-CC yielded diminutive specimens ascribed to *G. pliozea,* indicating Subzone SN12a. The absence of *G. pliozea* in Sample 189-1169A-21H-CC and its presence in Sample 22X-CC restricts the LO of this taxon (4.6 Ma) to between 198.19 and 202.06 mbsf. Planktonic foraminifers are common within Sample 189-1169A-22X-CC but are unusually small. Preservation within the *G. pliozea* Subzone is variable with many specimens exhibiting differing degrees of dissolution and abrasion.

Middle Miocene

Sample 189-1169A-22X-CC, which is assigned to the lower Pliocene, is underlain by sediments in Sample 189-1169A-23X-CC that contain specimens of *Paragloborotalia mayeri,* indicating an age of middle Miocene (Zone SN7). The presence of *P. mayeri* indicates a minimum age of 11.4 Ma for Sample 189-1169A-23X-CC. Thus, a significant stratigraphic gap (~6.8 m.y.) is inferred between Samples 189-1169A-22X-CC and 23X-CC. Preservation in Sample 189-1169A-23X-CC is good with abundant planktonic foraminifers.

Mixed Assemblages of Indeterminant Age

Sample 189-1169A-24X-CC contains a mixed assemblage; however, the presence of *Paragloborotalia continuosa* restricts the age to a minimum of Zone SN9 (8.0 Ma). Given its stratigraphic position, Sample 189-1169A-24X-CC should be relatively older than Sample 189-1169A-23X-CC, yet the age of this mixed assemblage remains equivocal. It is suspected that another hiatus separates Samples 189-1169A-23X-CC and 24X-CC.

Sample 189-1169A-25X-CC contains an enigmatic assemblage characteristic of the Pleistocene, consisting only of small specimens of *G. quinqueloba* and *G. glutinata.* Assemblages contained within Sample 189-1169A-26X-CC also consist of upsection contaminants. These two lowermost samples are assigned a general Neogene age. Preservation throughout this part of the record varies from good (Section 189-1169A-25X-CC) to poor (Section 189-1169A-26X-CC) with planktonic foraminifers being common. Age-significant events are summarized in Table T5.

T5. Planktonic foraminifer datum levels, Hole 1169A, p. 52.

Benthic Foraminifers, Ostracodes, and Bolboforma

Benthic foraminifers are generally well preserved, highly diverse, and abundant at this site (Fig. F6). Faunal assemblages suggest a paleodepth of 2000–4000 m (abyssal). Sample 189-1169A-1H-CC contains the low-oxygen indicator *Chilostomella oolina*. Deposition under moderate- to well-oxygenated bottom-water conditions is inferred from Samples 189-1169A-2H-CC through 23X-CC. The presence of *Melonis barleeanus* and *Melonis pompilioides* suggests a high flux of organic carbon in these samples. Samples 189-1169A-24X-CC through 26X-CC lack *M. barleeanus* and *M. pompilioides,* suggesting a lower flux of organic carbon in this interval. The transition from samples containing *Melonis* spp. to those which do not contain *Melonis* spp. coincides with the middle/upper Miocene hiatus/condensed interval (see Figs. F4, F6).

F6. Paleodepth and interpretation of bottom-water conditions, based on benthic foraminiferal assemblages, p. 33.

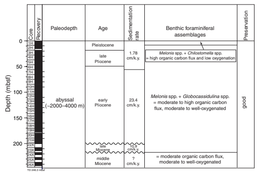

Other microfossils recorded include ostracodes, which are present throughout the drilled section. Their carapaces are mostly disarticulated, suggesting some degree of water turbulence. Additionally, bolboformids are present in Hole 1169A. *Bolboforma aculeata* is identified in Samples 189-1169A-22X-CC through 26X-CC. This species has a range from the base of Zone N14 to the top of Zone N17 at the Miocene/Pliocene boundary (Spiegler and von Daniels, 1991). Notable is the high abundance of bolboformids in Sample 189-1169A-26X-CC.

Radiolarians

Sediments from Hole 1169A contain Pliocene to middle Miocene "non-antarctic" and antarctic radiolarians. Abundant, well-preserved radiolarians were recovered from Samples 189-1169A-1H-CC through 17H-CC. Samples 189-1169A-18H-CC through 20H-CC commonly contain radiolarians, but with poor preservation. Samples 189-1169A-21H-CC through 25X-CC yield few to common radiolarians, whereas Sample 189-1169A-26X-CC is almost barren of radiolarians.

Samples 189-1169A-1H-CC through 11H-CC yield typical antarctic faunas. An abrupt faunal change to non-antarctic assemblages is present between Samples 189-1169A-11H-CC and 12H-CC. This fauna lacks or rarely contains species of *Antarctissa, Cycladophora,* and *Spongoplegma.* However, previous studies have reported rare to common occurrence of these taxa in the subantarctic near the Subtropical Convergence.

Pliocene

Radiolarian evidence suggests that the interval between Samples 189-1169A-1H-CC through 22X-CC should be assigned to the Pliocene. Sample 189-1169A-1H-CC is younger than the LO of *Eucyrtidium calvertense*. This sample is older than 1.9 Ma as indicated by the presence of *E. calvertense*. Five events are recognized for age assignment in the Pliocene interval (viz., the LO of *Pseudocubus vema* between Samples 189-1169A-4H-CC and 5H-CC (2.4 Ma), the LO of *Lampromitra coronata* between Samples 189-1169A-6H-CC and 7H-CC (3.35 Ma), the FO of *P. vema* between Samples 189-1169A-7H-CC and 8H-CC (4.5 Ma), the LO of *Lychnocanoma grande* between Samples 189-1169A-16H-CC and 17H-CC (5.0 Ma), and the LO of *Dictyophimus splendens* between Samples 189-1169A-21H-CC and 22X-CC (5.2 Ma). Samples 189-1169A-1H-CC through 4H-CC are correlated to the *E. calvertense* Zone, Samples 189-1169A-5H-CC through 7H-CC to the Upsilon Zone, and Samples 189-1169A-8H-CC through 11H-CC to the Tau Zone, respectively. The interval between Samples 189-1169A-12H-CC through 23X-CC cannot be correlated to any radiolarian zonal schemes, owing to the absence of zonal marker species.

Published records show that the FO of *Cycladophora davisiana* is found in the Upsilon Zone, but this species is present consistently from Samples 189-1169A-1H-CC through 11H-CC. This inconsistent stratigraphic distribution probably resulted from disturbance of sediments during coring.

Radiolarian assemblages from Samples 189-1169A-1H-CC through 11H-CC are characterized by the presence of antarctic or cold-water species, such as *C. davisiana, Cycladophora humerus, Cycladophora pliocenica, Cycladophora spongothorax, Spongoplegma antarcticum,* and *Triceraspyris antarctica*. The assemblage within this interval also contains species living in mid- to high-latitudes of the North Pacific such as *Sphaeropyle langii* and its ancestor *Sphaeropyle robusta.*

Radiolarian faunas change abruptly between Samples 189-1169A-11H-CC and 12H-CC. Antarctic or cold-water species become less abundant in Samples 189-1169A-12H-CC through 20H-CC, whereas spumellarians such as *Thecosphaera* become more abundant. These faunas are comparable to those in Samples 1168A-12H-CC through 20X-CC, with the exception that 20X-CC lacks any artiscinid species. The assemblages of Samples 189-1169A-12H-CC through 20H-CC occasionally contain a few specimens of antarctic or cold-water dwelling species.

Between Samples 189-1169A-20H-CC and 21H-CC there is a sharp decrease in species diversity. Radiolarians in Sample 189-1169A-21H-CC through 23X-CC consist mainly of *Stylacontarium acquilonium, Druppatractus irregularis, Hexacontium* spp., and *Thecosphaera* spp. Sample 189-1169A-22X-CC is marked by the common occurrence of reworked Miocene species such as *Cyrtocapsella japonica* and *Cyrtocapsella tetrapera.*

Middle Miocene

The upper Miocene is apparently missing from Hole 1169A based on radiolarian evidence. The interval represented by Samples 189-1169A-23X-CC through 25X-CC is assigned to the middle Miocene. The fauna is similar to that from the mid-latitude North Pacific with respect to the occurrence of *C. tetrapera, C. japonica, Lychnocanoma nipponica nipponica,* and *Theocorys redondoesnsis*. These species are dominant in the mid-latitude oceans.

One bioevent, the last abundant occurrence (LAO) of *C. tetrapera* is recognized between Samples 189-1169A-23X-CC and 24X-CC. This event occurred during 12.5 Ma in the North Pacific. Sample 189-1169A-26X-CC lacks age-diagnostic radiolarians.

Diatoms, Silicoflagellates, and Sponge Spicules

All core-catcher material from Hole 1169A was analyzed for diatoms, silicoflagellates, and sponge spicules. Smear slides were examined to assess overall relative abundance, and additional material was cleaned of the carbonate component for full assemblage analysis. Diatoms are present in common to high abundance in Cores 189-1169A-1H through 17H with good to moderate preservation. Notable, however, is Sample 189-1169A-14H-CC, which is almost completely barren of diatoms and sponge spicules. Sample 189-1169A-18H-CC and below contain rare to few diatoms in a poor to moderate state of preservation. Relative abundance data for diatoms, sponge spicules, and silicoflagellates are presented in Table **T6.**

Most biostratigraphic diatom markers (see **"Biostratigraphy,"** p. 9, in the "Explanatory Notes" chapter) are not present in core-catcher material from Hole 1169A. Some reworking is evident, notably in Sample 189-1169A-24X-CC, where upper Oligocene to lower Miocene material is inferred to be reworked into middle Miocene sediments by the common presence of the well-preserved late Oligocene to early Miocene marker *Rocella gelida* var. *gelida* and the variety *schraderi*. No other samples contain these taxa. Robust diatom *Actinocyclus ingens* var. *nodus* may also be reworked into Sample 189-1169A-24X-CC.

The LO of *Proboscia barboi* (1.8 Ma) is confidently placed within Core 189-1169A-1H. This defines the youngest bioevent for this site. Similarly, the LO of *Fragilariopsis weaveri* (2.6 Ma) and *Fragilariopsis lacrima* (2.9 Ma) are positioned between the two upper cores and Cores 189-169A-4H and 5H, respectively. An apparent FO of *Fragilariopsis barronii* (4.44 Ma) is encountered between Cores 189-1169A-6H and 7H, but this event is discarded from the final age model for reasons explained above. The LO of *A. fryxellae* (6.7 Ma) is present between Cores 189-1169A-20H and 21H. This robust taxon is observed in trace amounts in samples above Core 189-1169A-20H and is assumed to be reworked. The LO of the distinctive middle–late Miocene marker *Denticulopsis dimorpha* (10.7 Ma) is confidently placed between Cores 189-1169A-23X and 24X. Diatom datums are presented along with other microfossil events in Table **T7.**

T6. Relative abundance of selected diatom taxa, sponge spicules, and silicoflagellates, Hole 1169A, p. 53.

T7. Combined bioevents used for age model, Hole 1169A, p. 54.

Paleoceanographic information is evident from the initial analyses of diatom floras at Site 1169. Downhole floristic and diversity changes suggest fluctuations in the dominance of different water masses. Samples 189-1169A-1H-CC through 4H contain a relatively diverse, mixed flora of temperate-warm taxa (e.g., *Hemidiscus cuneiformis*) and endemic subantarctic-antarctic taxa (e.g., *Thalassiosira lentiginosa*). Samples 189-1169A-5H-CC and 8H-CC contain a comparatively lower diversity flora of dominantly temperate-warm species, whereas Samples 189-1169A-7H-CC and 13H-CC contain dominantly subantarctic-antarctic taxa. The remaining samples contain a mixed flora (viz., Samples 189-1169A-1H-CC through 4H; see above). Noteworthy, however, is the distinctive change from Samples 189-1169A-8H-CC (temperate-warm signal) to 7H-CC (subantarctic-antarctic signal) occurring at (inferred) 4.0 Ma in the late early Pliocene. Such changes may herald meridional shifts in the position of the Subtropical Convergence. Radiolarian and dinocyst assemblage changes observed at this site (see **"Radiolarians,"** p. 13, and **"Palynology,"** p. 15) also imply surface-water variations over this site.

Palynology

Onboard palynological analysis included approximately half of the core-catcher samples taken from Hole 1169A. Recovery of palynomorphs was good down to Sample 189-1169A-9H-CC, assigned to the earliest Pliocene on nannofossil evidence. Unfortunately, below this horizon, samples are barren or palynomorphs (notably dinoflagellate cysts) are present only in trace amounts. Such occurrences are considered the result of downhole contamination. Dinoflagellate cysts (dinocysts) are the most abundant palynomorphs in Hole 1169A; these occurrences represent the southernmost late Neogene dinocyst record ever found. Foraminifer organic linings and sporomorphs are the other quantitatively important categories of palynomorphs present in Hole 1169A (Table T8).

T8. Distribution of organic walled dinocysts and percentage of sporomorph and foraminifer linings, Hole 1169A, p. 55.

Middle Pleistocene to upper Pliocene Samples 189-1169A-1H-CC and 4H-CC yield relatively well-diversified dinocyst assemblages. Most abundant are taxa indicative of relatively warm, oligotrophic water masses. Also common are species that suggest the influence of distinctly colder and more eutrophic water masses. The latter include taxa endemic to the Antarctic region such as *Dalella chathamense* and *Selenopemphix antarctica.* In these "mixed" assemblages, cysts of presumed heterotrophic dinoflagellates (e.g., of *Protoperidinium* spp.) are also relatively common. Their occurrence may also be caused by the occasional presence of nutrient-rich surface waters, possibly associated with the "cold portion" of the assemblage. The mixed assemblages may indicate shifts of the position of the Subtropical Convergence (see **"Diatoms, Silicoflagellates, and Sponge Spicules,"** p. 14).

The underlying lower Pliocene Samples 189-1169A-5H-CC and 9H-C, in contrast, yield poorly diversified dinocyst assemblages generally indicative of warm oligotrophic surface waters. Only in Sample 189-1169A-9H-CC can some indication of the influence of colder water masses be found in the occurrences of the arctic species *Impagidinium pallidum* and the cold-temperate *Corrudinium harlandii*. The range top of *Invertocysta tabulata* (2.65 Ma) between Samples 189-1169A-5H-CC and 9H-CC may assist the age assessment of Hole 1169A (Table T9; Fig. F4).

T9. Selected age-diagnostic dinocyst event, Hole 1169A, p. 56.

Below Sample 189-1169A-9H-CC, available core-catcher samples are barren or yield a few dinocysts (usually *Nematosphaeropsis labyrinthea, Impagidinium aculeatum,* and/or *Impagidinium paradoxum*) that are quite abundant in the overlying interval. These taxa are stratigraphically long ranging and may be present in situ through to early Miocene age or even older sediments. However, given the problems with core recovery at Site 1169, these occurrences are considered a result of downhole contamination, rather than being in place.

Age Model and Sedimentation Rates

Because of the caving throughout the majority of Cores 189-1169A-1H to 21H, FO datums can not be placed with any confidence, therefore only the LO bioevents have been used in the final biostratigraphic assessment of Site 1169. These events total 19 and are presented in Table T7.

The age-depth curve is presented in Figure F4. The curve is refined by four paleomagnetic events in the Pliocene–Pleistocene (see **"Paleomagnetism,"** p. 17). Ages may be in error by as much as 1 m.y. at the base of Hole 1169A because of the lack of biostratigraphic data for the bottom three cores. Two hiatuses are inferred—one spanning the interval of 12.5–6.9 Ma (defined by the LAO of *C. tetrapera* and the LO of *A. delicatus,* respectively) and a second spanning the interval of 6.7–4.6 Ma (defined by the LO of *A. fryxellae* and *G. pliozea,* respectively). Unfortunately, the Miocene/Pliocene boundary falls within the younger hiatus. A short period of sedimentation (200 k.y.) at a rate of 10.9 cm/k.y. is inferred between the two periods of net nondeposition. Unfortunately, no definitive biostratigraphic information was recovered for Cores 189-1169A-8H through 16H. The age-depth model is most sketchy for this interval and should be regarded as such. However, one interpretation suggests a significant increase of nannoplankton production based on an apparently rapid (600 k.y.) and elevated sedimentation rate (23.4 cm/k.y.) in the lower Pliocene (4.6–4.0 Ma) following the younger hiatus. Increased calcareous nannoplankton production resulting in elevated sedimentation rates is observed in the lower Pliocene in tropical and temperate locations (Kennett and Von der Borch, 1986; Nelson, 1986); however, this phenomenon is recorded in the subantarctic for the first time. The average sedimentation rate in the upper Pliocene and Pleistocene falls to just 1.78 cm/k.y. The moderate amount of scatter in the bioevents during this period (Fig. F4) created problems for delineating an average sedimentation rate for this period. The curve, which is defined by the paleomagnetic events, conveniently approximates to an average through the scatter. It is stressed again that the age-depth model should be regarded with caution for intervals where the core is disturbed (see **"Lithostratigraphy,"** p. 6).

PALEOMAGNETISM

Introduction

After alternating-field (AF) demagnetization to 20 mT, the natural remanent magnetization (NRM) of whole-round sections from Hole 1169A was measured at 5-cm intervals using the pass-through cryogenic magnetometer. An exception was made for cores whose liners were deformed, to avoid possible damage to the magnetometer. These deformed sections were measured as archive-half cores. The nonmagnetic core barrel assembly was used for odd-numbered cores, starting with Core 3H. The comparison between results from cores collected with the nonmagnetic corer and those from the standard corer is discussed in the **"Appendix"** chapter as are results of experiments investigating the effect of core splitting on magnetization and other coring-related magnetic experiments. The Tensor tool was used to orient the APC cores beginning with the third core at each hole, but the variability in the declination values of the cores from Hole 1169A precluded the orientation of cores.

Discrete oriented samples were routinely collected from Hole 1169A; two samples were taken from each working-half core. These samples were used to aid in the interpretation of the long-core record of magnetization by providing additional measurements of polarity and basic magnetic characterization. Most of them were demagnetized at 5, 10, 15, 20, 30, 40, and 50 mT to permit principal component analysis. For rock magnetic characterization, anhysteretic remanent magnetization (ARM) was induced in 0.2-DC and 200-mT AC fields and isothermal remanent magnetization (IRM) in a DC field of 1 T. Some discrete samples were progressively saturated up to 1.3 T to study the hardness of the IRM.

Results

Long-Core Measurements

The long-core measurements were predominantly normal (Fig. F7) throughout the hole, which reflected the ubiquitous flow-in disturbance of the hole. The affected cores exhibit extreme deformation, with features extended in the upcore direction (see **"Lithostratigraphy,"** p. 6). The associated magnetization appears to be consistently upward. The sediment must therefore be remagnetized in the upward direction by the present field and then oversteepened so that the behavior is not

F7. Long-core results showing limited magnetostratigraphy for the late Pliocene and early Pleistocene, p. 34.

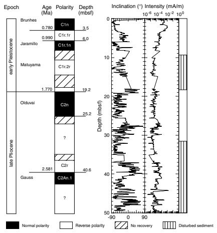

entirely passive, as in the passive markers of structural geology. The extreme upward inclination caused by the deformation serves as a useful marker of sediment plastic deformation.

Many core section extremities presented an anomalous reversal of inclination and intensity increase, part of which appears to record magnetic contamination during section cutting and capping. The strong remagnetization in the normal direction was helpful in the identification of contamination. It appeared important in carbonate sediments marked by a weak intensity on the order of 10^{-4} or 10^{-5} A/m. For the remaining sites of Leg 189, where weak intensities are also expected, this effect will have to be taken into consideration in evaluating the reliability of apparent short reversal chrons at the ends of sections.

Sequences of poorly recorded reversals appeared in the upper part of Hole 1169A, where no flow-in was observed (Fig. F7). With the help of biostratigraphic datums (see "Biostratigraphy," p. 9), these reversals were identified as being the onset of Brunhes Chron (C1n) at 3.5 mbsf, the termination of Jaramillo Subchron (C1r.1n) at 6 mbsf, the Olduvai Subchron (C2n) between 19.2 and 25.2 mbsf, and the termination of Subchron C2An.1r at 40.6 mbsf.

Discrete Samples

Most of the progressive demagnetization carried out on discrete samples did not permit identification of reliable paleodirections of the magnetic field. The NRM, ARM, and IRM values and NRM:IRM ratio suggest a detrital origin of the magnetic signal (Fig. F8). Among these cores, Core 189-1169A-22X was marked by a microtektites layer (see "Lithostratigraphy," p. 6). Rock magnetic analysis on discrete samples taken from Core 189-1169A-22X confirmed this observation. The ratio of ARM:IRM is high, indicating that the magnetic signal is principally carried by fine particles. The sediment containing the microtektites has acquired a stable magnetization (Fig. F8), that is considerably stronger than other sediments. The presence of microtektites, revealed by this relatively strong intensity, is apparent between 198.5 and 212.2 mbsf. This suggests that the microtektites were initially magnetized and have been magnetically oriented in the past field direction. Microscope observations showed spherical microtektites ~200 µm in diameter. The particles are likely to carry a thermoremanent magnetization acquired during initial cooling that is evidently strong enough to orient them in the water column and in the final sediment.

F8. Magnetic characteristics for two samples, p. 35.

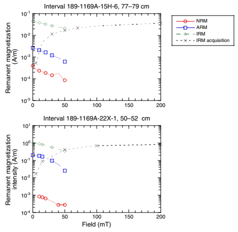

Magnetostratigraphy

A reliable magnetostratigraphy could not be established at this site because of the extreme sediment deformation (Fig. F7). The few chrons recognized in the upper part of Hole 1169A (Fig. F8) were dependent upon biostratigraphic tie points (Table T10). Reversed magnetizations are observable at the ends of some sections. But, we did not interpret them because of the sensitivity of these weakly magnetized carbonates to magnetic contamination, which appears to be concentrated at the end of cores. Discrete-sample demagnetization revealed a poor magnetic record, so that even in the absence of the deformation, it would probably have proved difficult to obtain a good magnetostratigraphy.

T10. Magnetostratigraphic results, p. 57.

ORGANIC GEOCHEMISTRY

The shipboard organic geochemistry program at Site 1169 included studies of volatile hydrocarbons, total nitrogen, and total organic and inorganic carbon. CNS analysis, gas chromatography, and carbon coulometry were performed (see **"Organic Geochemistry,"** p. 20, in the "Explanatory Notes" chapter). Sample spacing varied because of the core disturbance during drilling; therefore, a lower resolution geochemical record was produced here compared to Site 1168.

Sedimentary Geochemistry

Results

Carbonate ($CaCO_3$) content values for the strata sampled at Site 1169 range from 60 to 95 wt% (Fig. F9; Table T11). In general, the profile exhibits an overall slightly decreasing upward trend. Sediments from ~250 to ~170 mbsf commonly contain >90 wt% $CaCO_3$, except for one horizon with a value of ~85 wt%. An abrupt decrease to ~60 wt% is observable at ~135 mbsf. From this horizon, carbonate content values fluctuate between ~80 and 90 wt%.

F9. Plots of carbonate, total organic carbon, total nitrogen, and C/N ratios, Hole 1169A, p. 36.

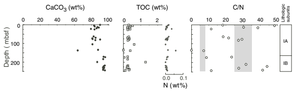

The total organic carbon (TOC) content for most samples from Site 1169 is <0.7 wt%, except for one sample at ~200 mbsf that contains >1.3 wt% TOC (Fig. F9; Table T11). Organic matter type was assessed using C and N analyses (Fig. F9; Table T11); C/N ratios of ~5–8 are generally considered as indicative of marine organic matter, whereas ratios of ~25–35 suggest the presence of terrestrially derived organic matter (Bordovskiy, 1965; Emerson and Hedges, 1988). Total nitrogen content through the core is generally low, so C/N ratios must be considered with care.

T11. Values for inorganic carbon, calcium carbonate, total carbon, total organic carbon, total nitrogen, and C/N in sediments, Hole 1169A, p. 58.

Discussion

The high carbonate content of sediments at Site 1169 reflects a dominance of calcareous nannoplankton and foraminifers (see **"Biostratigraphy,"** p. 9). The extremely high carbonate content may represent enhanced carbonate preservation, perhaps indicating relatively high biogenic productivity. This observation is similar to one made for middle Miocene through Quaternary sediments at Site 1168. Of note is the carbonate decline at ~135 mbsf. Several distinct carbonate declines are visible between ~100 and 200 mbsf at Site 1168 (see Fig. F27, p. 87, in the "Site 1168" chapter), so these horizons with relatively low carbonate content may represent regionally correlatable horizons.

The generally low TOC contents in this sequence seem to record settling of organic matter through a well-mixed water column and/or to a well-oxygenated seafloor. The TOC content profile here is similar to the TOC content distribution at Site 1168, even considering the lower resolution sampling at Site 1169. Of particular interest are the TOC content variations between ~100 and 200 mbsf (Fig. F9), which are similar to variations observed between ~60 and 160 mbsf in Hole 1168A (see Fig. F27, p. 87, in the "Site 1168" chapter). These peaks may represent similarities in organic carbon preservation recorded at both sites.

The C/N ratios show a wide range of values from 0 to >100 and covary with the TOC content. Some of these apparent variations may be described by the extremely low total nitrogen content of the samples. However, if these values indicate variations in organic matter type, then they may record variations in seafloor redox conditions. Low C/N intervals could record preservation of marine-derived organic matter perhaps associated with carbonate producers, or dinoflagellates (see **"Biostratigraphy,"** p. 9), whereas relatively higher C/N intervals may record organic matter denitrification. Denitrification is usually limited in marine sediments (Killops and Killops, 1994) and does not generally occur until most of the sedimentary organic carbon has been metabolized (Mechalas, 1974). Alternatively, the high C/N units may represent total oxidation of labile-marine organic matter and subsequent preservation of minor quantities of refractory terrestrial residuum.

Volatile Hydrocarbons

Results

Concentrations of volatile hydrocarbon gases were measured from every core using the standard ODP headspace-sampling technique and gas chromatographic analysis. Methane content (Table **T12**) was extremely low (0 to <100 ppmv), although it generally increases downcore.

Discussion

The extremely low gas content at Site 1169 is likely a function of two characteristics of the sediment. First, the sediments contain little organic matter as a source of natural gas. Second, pore-water profiles show that appreciable SO_4^{2-} exists to the bottom of Hole 1169A; thus, sulfate reduction processes may be limiting the onset of methanogenesis in this interval (see **"Inorganic Geochemistry,"** p. 20).

INORGANIC GEOCHEMISTRY

Shipboard interstitial water (IW) analyses were performed on 15 of the 27 whole-round samples taken from Hole 1169A. The balance of the samples was archived for shore-based investigations. The whole-round samples were taken at the frequency of three per core in the upper ~70 mbsf, one per core from 70–100 mbsf, and one every third core to total depth. All results on IW geochemistry are reported in Table **T13** and Figures **F10, F11, F12, F13,** and **F14.** Although the sediment cores were heavily disturbed during drilling, the geochemical results on IW exhibit patterns that are comparable to those obtained at Site 1168.

Chloride, Sodium, and Salinity

The conservative parameters salinity (not shown in figure), chloride (Cl^-), and sodium (Na^+) exhibit very little change within the upper 250 mbsf (Fig. **F10**). Salinity decreases downward to 34 from the near-seafloor concentration of ~35; maximum dilution relative to seawater is only 3%. Chloride varies from 556 to 564 mM and exhibits a maximum at ~25–50 mbsf. Sodium ranges between 470 and 488 mM and remains conservative with respect to Cl^-. Within the analytical precision of shipboard instrumentation, the Na^+ concentrations show no change with depth from the normal seawater sodium concentration of 480 mM.

The ~1.4% increase in chloride within the upper ~25–50 mbsf relative to the uppermost sample, which was also observed in Hole 1168,

T12. Headspace gas composition, Hole 1169A, p. 59.

T13. Interstitial water data, Hole 1169A, p. 60.

F10. Concentration-depth profiles of Cl^- and Na^+, p. 37.

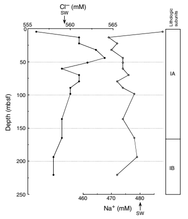

F11. Concentration-depth profiles of SO_4^{2-}, pH, and alkalinity, p. 38.

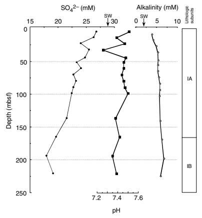

F12. Concentration-depth profiles of Sr^{2+}, Ca^{2+}, and Li^+, p. 39.

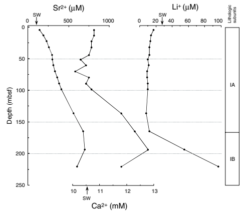

F13. Concentration-depth profiles of Mg^{2+} and K^+, p. 40.

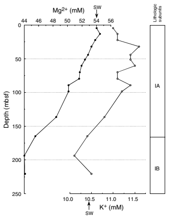

may be attributed to a salinity increase during the last glacial maximum as proposed by McDuff (1985) and Schrag et al. (1996).

F14. Concentration-depth profile of dissolved silica within interstitial water, p. 41.

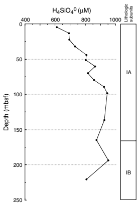

Sulfate, pH, and Alkalinity

Titration alkalinity values from the uppermost pore waters are ~4.0 mM and slightly increase to a maximum of 6.8 mM at ~200 mbsf (Fig. **F11**). The pH decreases from ~7.5 at the top to <7.3 at 30 mbsf and subsequently increases to 7.5 between 40–100 mbsf (Fig. **F11**). From that depth downward, the pH continuously decreases to <7.4. Sulfate concentrations decrease from near-seawater values (26–27 mM) at the top of the hole to a minimum of ~18 mM at ~200 mbsf (~33% decrease), thus never being completely removed (Fig. **F11**).

The downcore change in sulfate and alkalinity is most likely caused by organic matter remineralization. Interstitial water SO_4^{2-} concentrations at Site 1169 do not exhibit the same amount of depletion through comparable depths at Site 1168; the degree of sulfate reduction is half that observed at Site 1168, although TOC concentrations have comparable concentrations. The downcore change in alkalinity is similar at both holes, although values are generally lower by ~1–2 mM at Site 1169.

Strontium, Calcium, and Lithium

Strontium (Sr^{2+}) concentrations gradually increase with depth from ~141 µM near the seafloor to ~700 µM at 200 mbsf (Fig. **F12**). A Sr^{2+} concentration decline to ~600 µM was observed from 200 mbsf to the base of the hole. Calcium (Ca^{2+}) concentrations remain near seawater values for the upper ~100 mbsf of the hole (Fig. **F12**). A distinct maximum in Ca^{2+} concentrations (12.8 mM) exists at ~200 mbsf. Lithium (Li^+) concentrations remain relatively constant with depth, varying between 8 and 17 µM in the uppermost ~170 mbsf (Fig. **F12**). Below, Li^+ concentrations steadily increase, reaching 97 µM at ~220 mbsf.

The pronounced maximum in Sr^{2+} concentrations at ~200 mbsf within the calcareous lithostratigraphic Unit I compares to the Sr^{2+} maximum at comparable depths in Hole 1168A, although absolute concentrations are higher in Hole 1168A. Recrystallization of biogenic calcite to diagenetic low-Mg calcite and dolomite and/or dissolution of biogenic calcite causes a release of dissolved strontium into pore waters (Manheim and Sayles, 1974; Baker et al., 1982). Dissolution and precipitation reactions were shown to control the Ca^{2+} profile at Site 1168. The increase in Li^+ in the same interval may also be attributed to alteration of biogenic carbonate, although the abundance of Li^+ in biogenic carbonates may not be sufficient to account for all the Li^+ observed here. Alternatively, the early diagenesis of biogenic opal-A and ion-exchange reactions involving clay minerals may influence dissolved Li^+ concentrations (Gieskes, 1983; DeCarlo, 1992).

Magnesium and Potassium

The downcore magnesium (Mg^{2+}) and potassium (K^+) profiles exhibit gradually decreasing concentrations (Fig. **F13**). Mg^{2+} concentrations are ~54 mM at the top of the hole and decrease by ~20% to ~44 mM at the base of Hole 1169A. K^+ concentrations decrease by ~10% in the hole. The change in concentration of both elements is highly correlated (r =

0.81) and suggests the involvement of similar processes (e.g., basement alteration, ion-exchange reactions associated with clay minerals; see Gieskes, 1983; De Carlo, 1992).

Silica

Dissolved silica concentrations ($H_4SiO_4^0$) range from ~600 to 950 µM and exhibit a near-continuous increasing downward profile (Fig. **F14**). The highest concentrations (>900 µM) are between ~90 and 190 mbsf. Below this, silica concentrations decrease to ~800 µM.

Although dissolved silica concentrations in Hole 1169A are consistently higher by ~20%–30% than those observed in Hole 1168A, the downcore pattern of dissolved silica is similar for the uppermost sediment sections in both cores. In Hole 1168A most silica dissolution occurs in sediments rich in biogenic silica and IW-silica concentrations are a reflection of the opal content of the sediments. In Hole 1169A, we expect a similar relationship between dissolved silica and biogenic opal. The suspected opal increase in Hole 1169A matches the observation that carbonate concentrations in Hole 1169A are slightly lower in lithostratigraphic Subunits IA and IB compared to Hole 1168A.

Geochemical Zonation

The pore-water profiles allow us to differentiate the cored interval into two geochemical zones. Lithostratigraphic Subunit IA is divided into an upper Zone 1 covering the upper ~100 mbsf. This zone contains no gradient in Ca^{2+} and K^+ concentrations, whereas dissolved silica is continuously decreasing. Zone 2, from ~100 to ~170 mbsf (the boundary between lithostratigraphic Subunits IA and IB), instead shows sharply increasing gradients in Ca^{2+} and K^+ concentrations, whereas dissolved silica reaches a steady state.

PHYSICAL PROPERTIES

The physical properties program at Site 1169 included multisensor track (MST) and thermal conductivity measurements of whole-round cores and compressional wave (*P*-wave) velocity, moisture and density (MAD), and vane shear-strength measurements of split cores. Because of the extensive disturbance of the cores and the pervasive flow-in, the quality of sediments recovered is poor and the available physical properties data set is limited.

Multisensor Track

All core sections from Hole 1169A were measured on the MST (for magnetic susceptibility, *P*-wave velocity, and gamma-ray attenuation [GRA] density) at 2-cm intervals. *P*-wave velocities were recorded at 2-cm intervals in Hole 1169A to a depth of ~197.9 mbsf. *P*-wave velocities were not recorded in the XCB-cored sections.

The combination of flow-in and high carbonate content of the sediments is reflected in the relatively unvarying downcore magnetic susceptibility profile (Fig. **F15A**). GRA density values and discrete wet bulk-density data exhibit similar downhole trends (Fig. **F15B**). The GRA and MAD density data, however, show more variability than the magnetic susceptibility data. Because of the ubiquitous flow-in, it is difficult to

F15. Magnetic susceptibility, GRA density, and discrete wet bulk density vs. depth, Hole 1169A, p. 42.

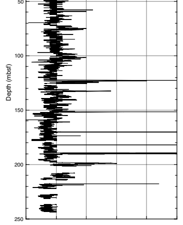

determine whether the downcore variations result from lithologic variation or disturbance. A significant decrease in GRA density at ~200 mbsf corresponds to the switch from APC to XCB coring.

GRA values are higher than the discrete density values (Fig. **F15B**) reflecting the MST calibration procedure. The calibration procedure for the MST is optimized for mixed sediments, so the GRA-density measurements are overestimated in the carbonate-rich sediments at Site 1169.

Velocity

Discrete compressional velocity measurements (PWS1, PWS2, and PWS3) were performed at a sample frequency of one per section, when sections were not characterized completely by flow-in or disturbed sediments (Fig. **F16;** Table **T14**). A comparison of the filtered continuous MST velocity profile with the discrete values is shown in Figure **F16.** PSW3 (x- [across core] direction) velocities are higher than expected for the sediment type (Fig. **F16**). The velocity measurements perpendicular (PSW1; z- [along core] direction) and parallel to the bedding (PSW2; y- [perpendicular to the core] direction) are similar, ranging between 1500 and 1620 m/s. Although discrete velocity measurements were always attempted in less disturbed intervals, data interpretation is difficult because of the high degree of disturbance and presence of flow-in throughout much of the core.

Vane Shear Strength

Vane shear strength was measured in sections with relatively low amounts of flow-in and disturbance in Hole 1169A. However, the data quality is unknown considering the high degree of disturbance. The shear strength results are displayed in Figure **F17** and Table **T15.** With the exception of several high shear-strength values at ~80 mbsf, the data fluctuate around an average of ~20 kPa.

Thermal Conductivity

Thermal conductivity was measured on Section 3 of Cores 1H–6H and 14H–18H in Hole 1169A (Fig. **F18;** Table **T16**). Thermal conductivity measurements are made before core splitting; therefore, it is impossible to assess sediment quality when taking measurements. The data are limited and of suspect quality because of the highly disturbed sediments and the presence of flow-in.

Moisture and Density

The density data from discrete samples (Fig. **F19;** Table **T17**) have a strong first-order correlation with the GRA data (Fig. **F15B**). MAD samples were chosen only from sections that appeared to display minimal disturbance or flow-in. However, because flow-in and disturbance were so prevalent, it is difficult to assess the quality of the data.

F16. *P*-wave velocities measured for discrete samples and in whole cores vs. depth, p. 44.

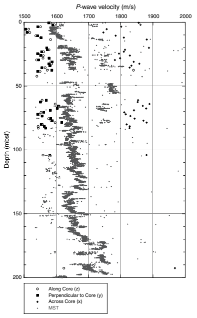

T14. *P*-wave velocities measured at discrete intervals, Hole 1169A, p. 61.

F17. Shear strength measured on whole cores vs. depth, Hole 1169A, p. 45.

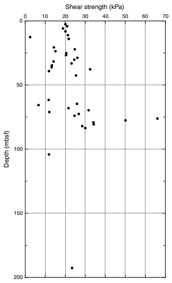

T15. Undrained shear strength from miniature vane-shear measurements, Hole 1169A, p. 62.

F18. Thermal conductivity measured on whole cores vs. depth, p. 46.

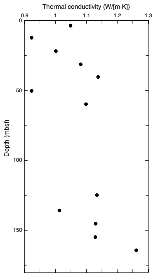

T16. Thermal conductivity measured on whole-core sections, Hole 1169A, p. 63.

F19. Wet bulk density, water content, and porosity measured at discrete intervals vs. depth, Hole 1169A, p. 47.

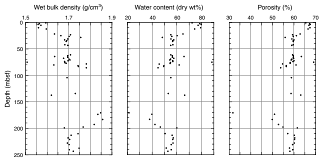

T17. Index properties measured at discrete intervals, Hole 1169A, p. 64.

REFERENCES

Baker, P.A., Gieskes, J.M., and Elderfield, H., 1982. Diagenesis of carbonates in deep-sea sediments: evidence from Sr^{2+}/Ca^{2+} ratios and interstitial dissolved Sr^{2+} data. *J. Sediment. Petrol.,* 52:71–82.

Barrows, T.T., Juggins, S., DeDeckker, P., Thiede, J., and Martinez, J.I., 2000. Sea-surface temperatures of the southwest Pacific Ocean during the Last Glacial Maximum. *Paleoceanography,* 15:95–109.

Berggren, W.A., Kent, D.V., Swisher, C.C., III, and Aubry, M.-P., 1995. A revised Cenozoic geochronology and chronostratigraphy. *In* Berggren, W.A., Kent, D.V., Aubry, M.-P., and Hardenbol, J. (Eds.), *Geochronology, Time Scales and Global Stratigraphic Correlation.* Spec. Publ.—Soc. Econ. Paleontol. Mineral. (Soc. Sediment. Geol.), 54:129–212.

Bordovskiy, O.K., 1965. Accumulation and transformation of organic substances in marine sediment, 2. Sources of organic matter in marine basins. *Mar. Geol.,* 3:5–31.

Boyle, E.A., and Keigwin, L.D., 1985. Comparison of Atlantic and Pacific paleochemical records for the last 215,000 years: changes in deep-ocean circulation and chemical inventories. *Earth Planet. Sci. Lett.,* 76:135–150.

Broecker, W.S., Peng, T.H., and Engh, R., 1980. Modeling the carbon system. *Radiocarbon,* 22:565–598.

Charles, C.D., Lynch-Stieglitz, J., Ninnemann, U.S., and Fairbanks, R.G., 1996. Climate connections between the hemispheres revealed by deep sea sediment core/ice core correlations. *Earth Planet. Sci. Lett.,* 142:19–27.

De Carlo, E.H., 1992. Geochemistry of pore water and sediments recovered from the Exmouth Plateau. *In* von Rad, U., Haq, B.U., et al., *Proc. ODP, Sci. Results,* 122: College Station, TX (Ocean Drilling Program), 295–308.

Emerson, S., and Hedges, J.I., 1988. Processes controlling the organic carbon content of open ocean sediments. *Paleoceanography,* 3:621–634.

Exon, N.F., Moore, A.M.G., and Hill, P.J., 1997. Geological framework of the South Tasman Rise, south of Tasmania, and its sedimentary basins. *Aust. J. Earth Sci.,* 44:561–577.

Flower, B.P., and Kennett, J.P., 1995. Middle Miocene deepwater paleoceanography in the southwest Pacific: relations with East Antarctic ice sheet development. *Paleoceanography,* 10:1095–1112.

Gartner, S., 1992. Miocene nannofossil chronology in the North Atlantic, DSDP Site 608. *Mar. Micropaleontol.,* 18:307–331.

Gieskes, J.M., 1983. The chemistry of interstitial waters of deep-sea sediments: interpretation of deep-sea drilling data. *In* Riley, J.P., and Chester, R. (Eds.), *Chemical Oceanography* (Vol. 8): London (Academic), 221–269.

Heath, R.A., 1985. A review of the physical oceanography of the seas around New Zealand–1982. *N. Z. J. Mar. Freshwater Res.,* 19:70–124.

Howard, W.R., and Prell, W.L., 1992. Late Quaternary surface circulation of the southern Indian Ocean and its relationship to orbital variations. *Paleoceanography,* 7:79–117.

Kennett, J.P., and von der Borch, C.C., 1986. Southwest Pacific Cenozoic paleoceanography. *In* Kennett, J.P., von der Borch, C.C., et al., *Init. Repts. DSDP,* 90 (Pt. 2): Washington (U.S. Govt. Printing Office), 1493–1517.

Killops, S.D., and Killops, V.J., 1994. *An Introduction to Organic Geochemistry:* Essex (Longman Scientific and Technical).

Manheim, F.T., and Sayles, F.L., 1974. Composition and origin of interstitial waters of marine sediments, based on deep sea drill cores. *In* Goldberg, E.D. (Ed.), *The Sea* (Vol. 5): *Marine Chemistry: The Sedimentary Cycle:* New York (Wiley), 527–568.

McDuff, R.E., 1985. The chemistry of interstitial waters, Deep Sea Drilling Project Leg 86. *In* Heath, G.R., Burckle, L.H., et al., *Init. Repts. DSDP,* 86: Washington (U.S. Govt. Printing Office), 675–687.

Mechalas, B.J., 1974. Pathways and environmental requirements for biogenic gas production in the ocean. *In* Kaplan, I.R. (Ed.), *Natural Gases in Marine Sediments*. Mar. Sci., 3:11–25.

Mortlock, R.A., Charles, C.D., Froelich, P.N., Zibello, M.A., Saltzman, J., Hays, J.D., and Burckle, L.H., 1991. Evidence for lower productivity in the Antarctic Ocean during the last glaciation. *Nature,* 351:220–223.

Nelson, C.S., 1986. Lithostratigraphy of Deep Sea Drilling Project Leg 90 drill sites in the Southwest Pacific: an overview. *In* Kennett, J.P., von der Borch, C.C., et al., *Init. Repts. DSDP,* 90: Washington (U.S. Govt. Printing Office), 1471–1491.

Rintoul, S.R., Donguy, J.R., and Roemmich, D.H., 1997. Seasonal evolution of upper ocean thermal structure between Tasmania and Antarctica. *Deep-Sea Res.,* 44:1185–1202.

Schrag, D.P., Hampt, G., and Murray, D.W., 1996. Pore fluid constraints on the temperature and oxygen isotopic composition of the glacial ocean. *Science,* 272:1930–1932.

Shipboard Scientific Party, 1999. Leg 177 summary: Southern Ocean paleoceanography. *In* Gersonde, R., Hodell, D.A., Blum, P., et al., *Proc. ODP, Init. Repts.,* 177: College Station, TX (Ocean Drilling Program), 1–67.

Sikes, E.L., 1995. Southern Ocean paleoceanographic studies: clues for changes in atmospheric CO_2 content. *In* Exon, N.F., et al. (Eds.), *AGSO Cruise 147 Report.* AGSO Record, 1995/56.

Spiegler, D., and von Daniels, C.H., 1991. A stratigraphic and taxonomic atlas of *Bolboforma* (Protophytes, incertae sedis, Tertiary). *J. Foraminiferal Res.,* 21:126–158.

Tchneria, P., 1980. *Descriptive Regional Oceanography:* New York (Pergamon Press).

Williams, G.L., Brinkhuis, H., et al., 1998. Cenozoic dinocyst events. *In* De Graciansky, et al. (Eds.), *Sequence Stratigraphy of European Basins*. Spec. Publ.—Soc. Econ. Paleontol. Mineral., 60.

Woodruff, F., and Savin, S.M., 1989. Miocene deepwater oceanography. *Paleoceanography,* 4:87–140.

Figure F1. A portion of seismic line *Tasmante* 125-04 through Site 1169, including the approximate depth of penetration. SP = shotpoint.

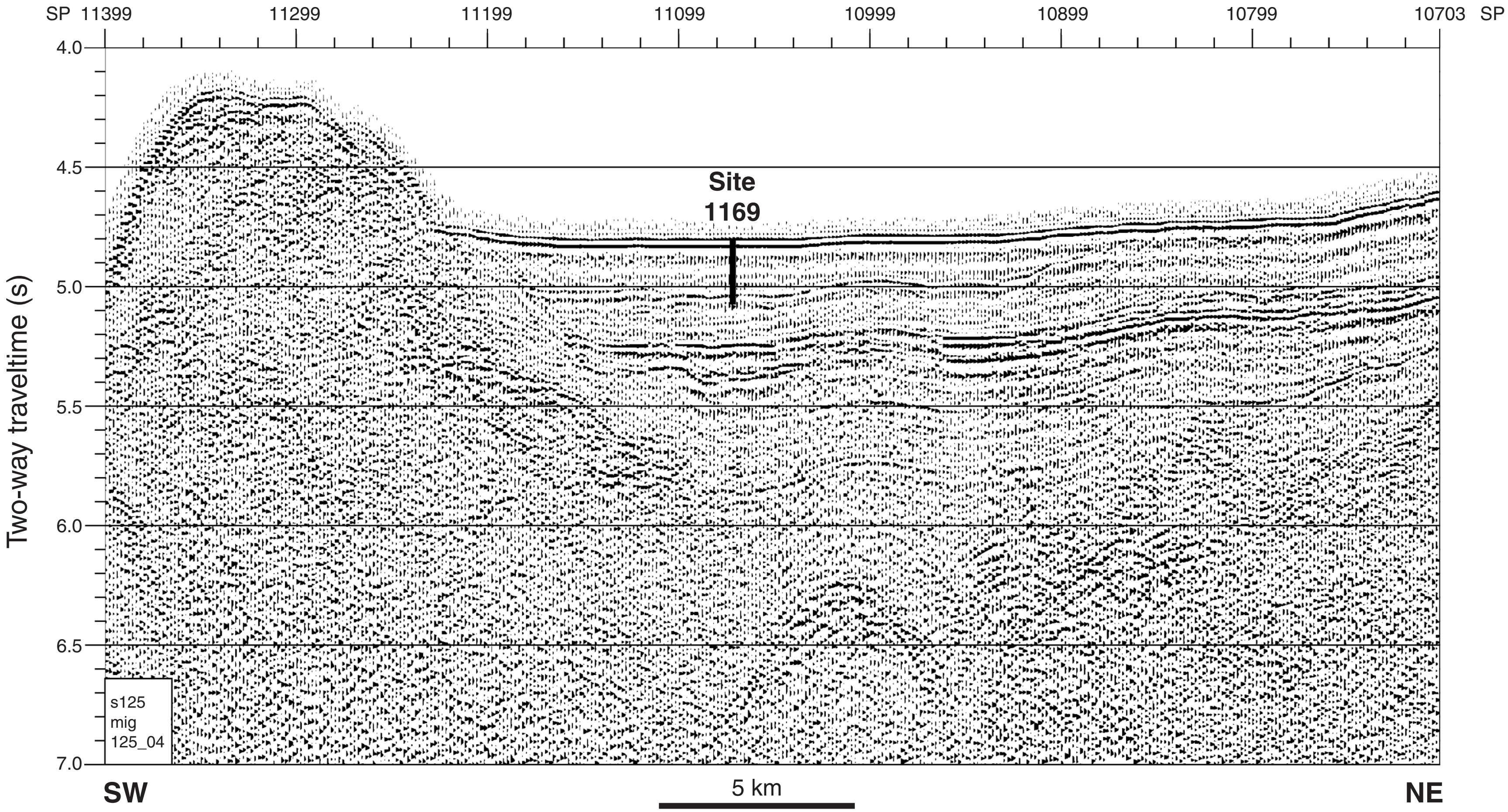

Figure F2. Lithostratigraphic summary of Site 1169, western South Tasman Rise. Magnetic susceptibility and GRA bulk-density profiles are not plotted in this summary figure, the quality of data being questionable because of the coring disturbances. TD = total depth.

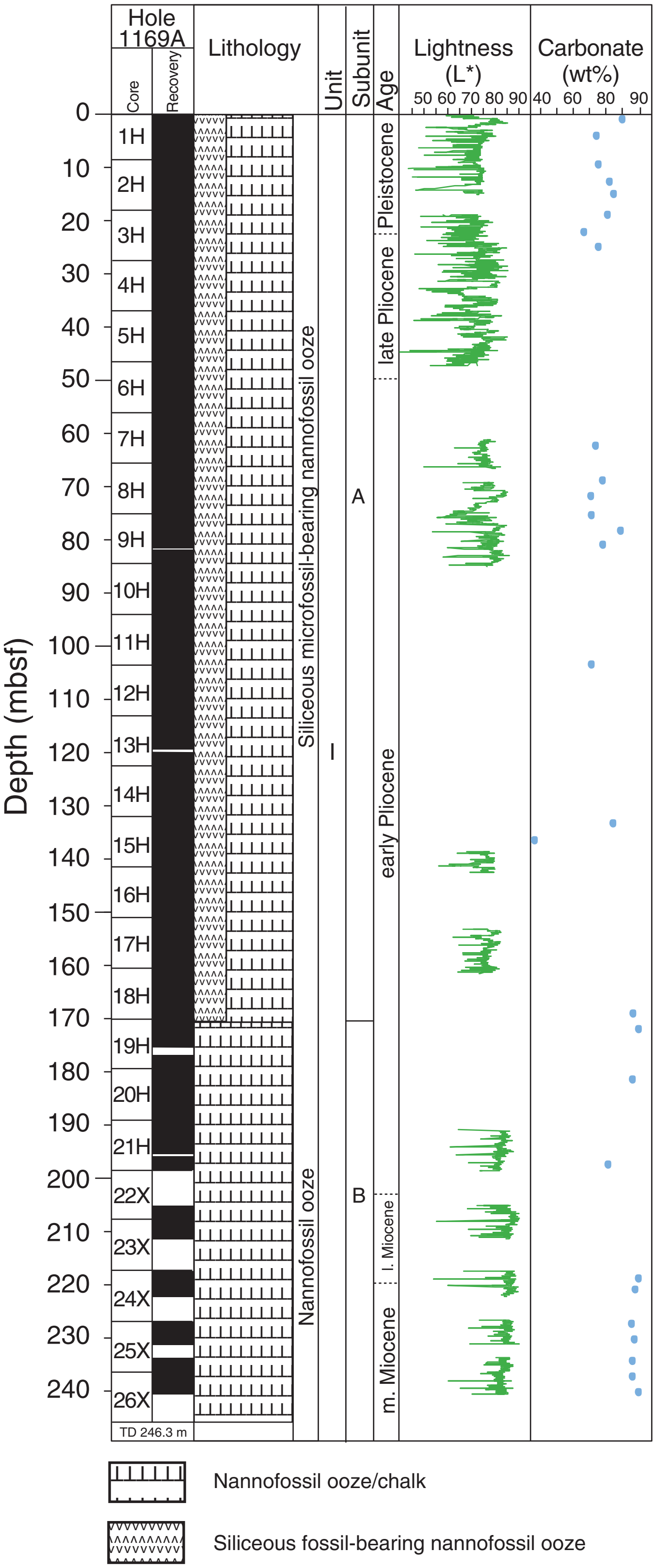

Figure F3. Physical and chemical properties of Site 1169. **A.** Relative sediment disturbance from 0 (no disturbance) to 4 (soupy or vertically deformed). **B.** Colorimetric coordinate b* by spectrophotometry (blue to negative and yellow to positive values). **C.** Calcium carbonate content in weight percent (see **"Organic Geochemistry,"** p. 19). **D.** Relative abundance of siliceous and calcareous microfossils as identified in smear slides, standardized against calcium carbonate content. Nonbiogenic components, such as clays and in situ minerals, are generally in low abundance (~10%) and are not considered in this diagram. TD = total depth. (**Figure shown on next page.**)

Figure F3 (continued). (Caption shown on previous page.)

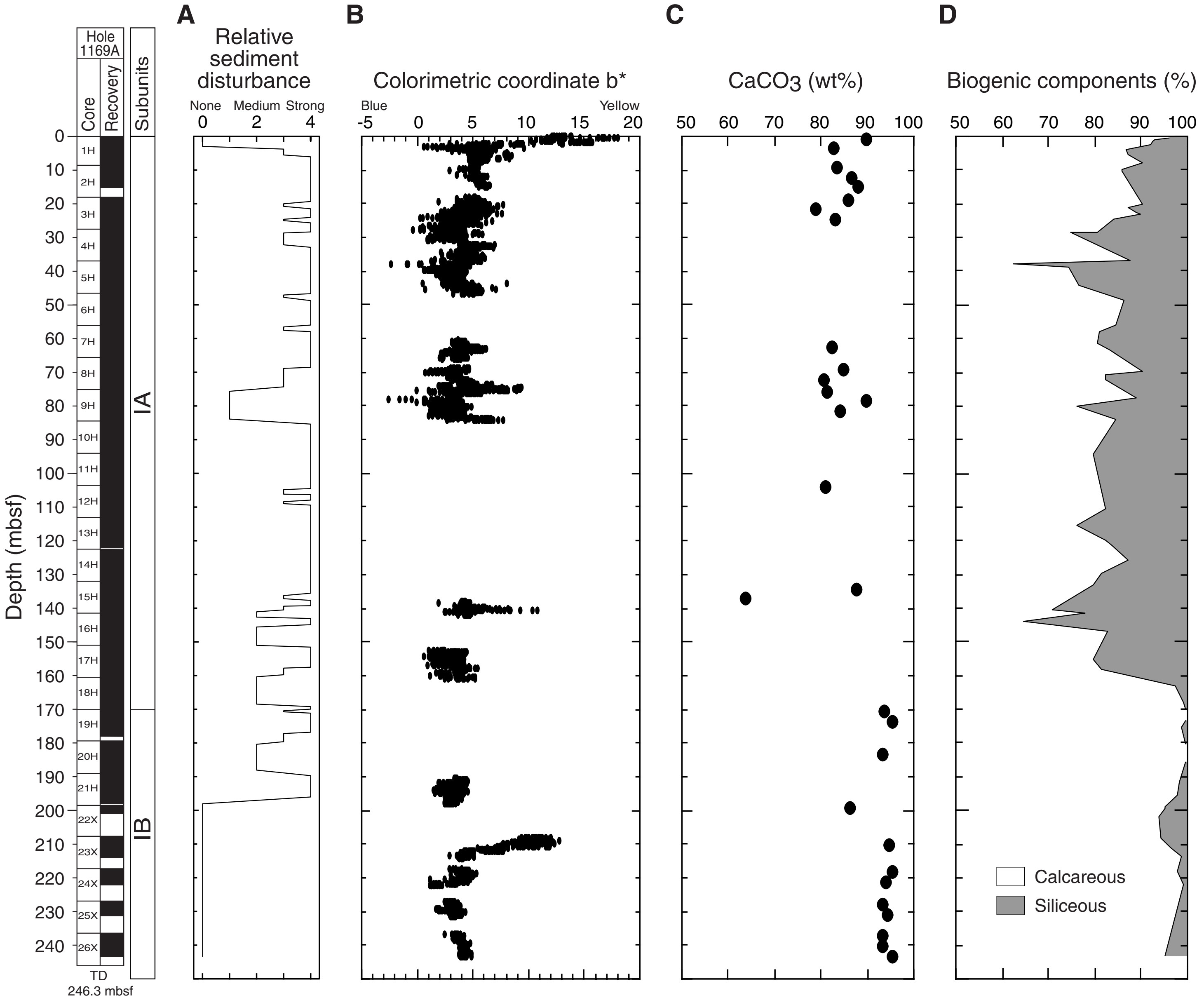

Figure F4. Site 1169 age-depth plot and linear sedimentation rates. Note that widespread core disturbance means that this plot should be regarded with caution.

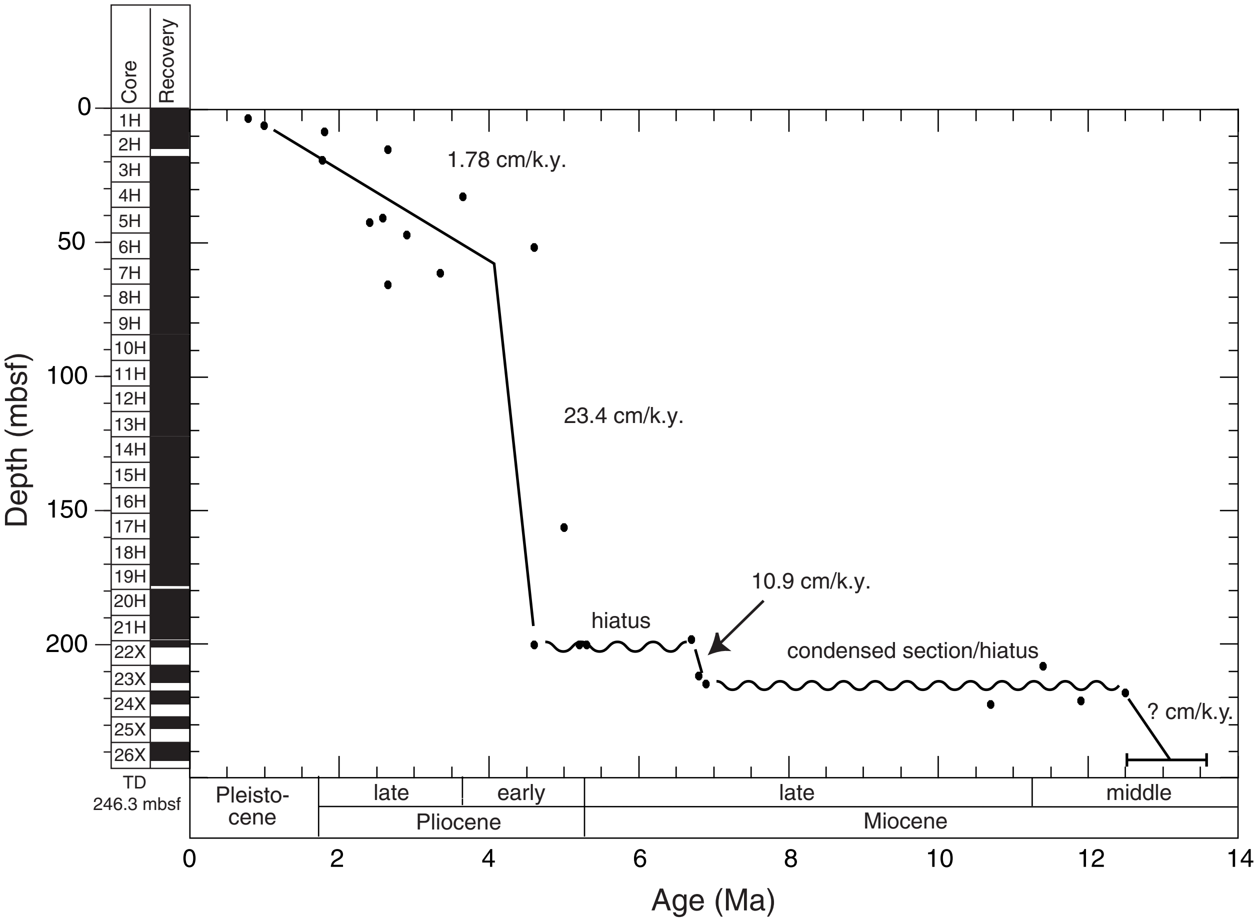

Figure F5. Color changes associated with water temperature shift (interval 189-1169A-23X, 110–140 cm).

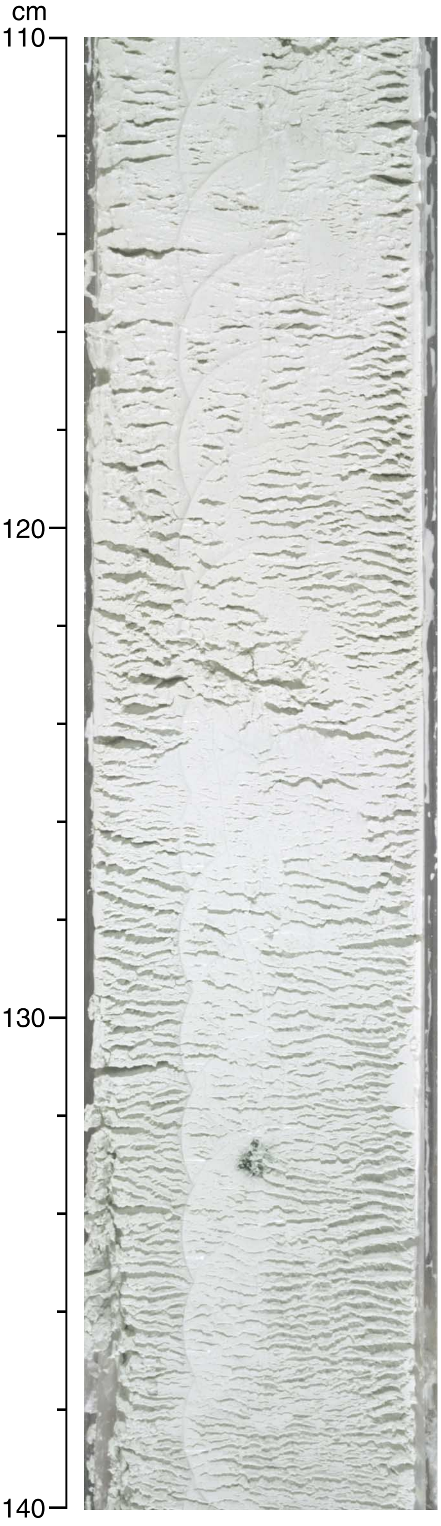
cm
110
120
130
140

Figure F6. Paleodepth and interpretation of bottom-water conditions, based on benthic foraminiferal assemblages. TD = total depth.

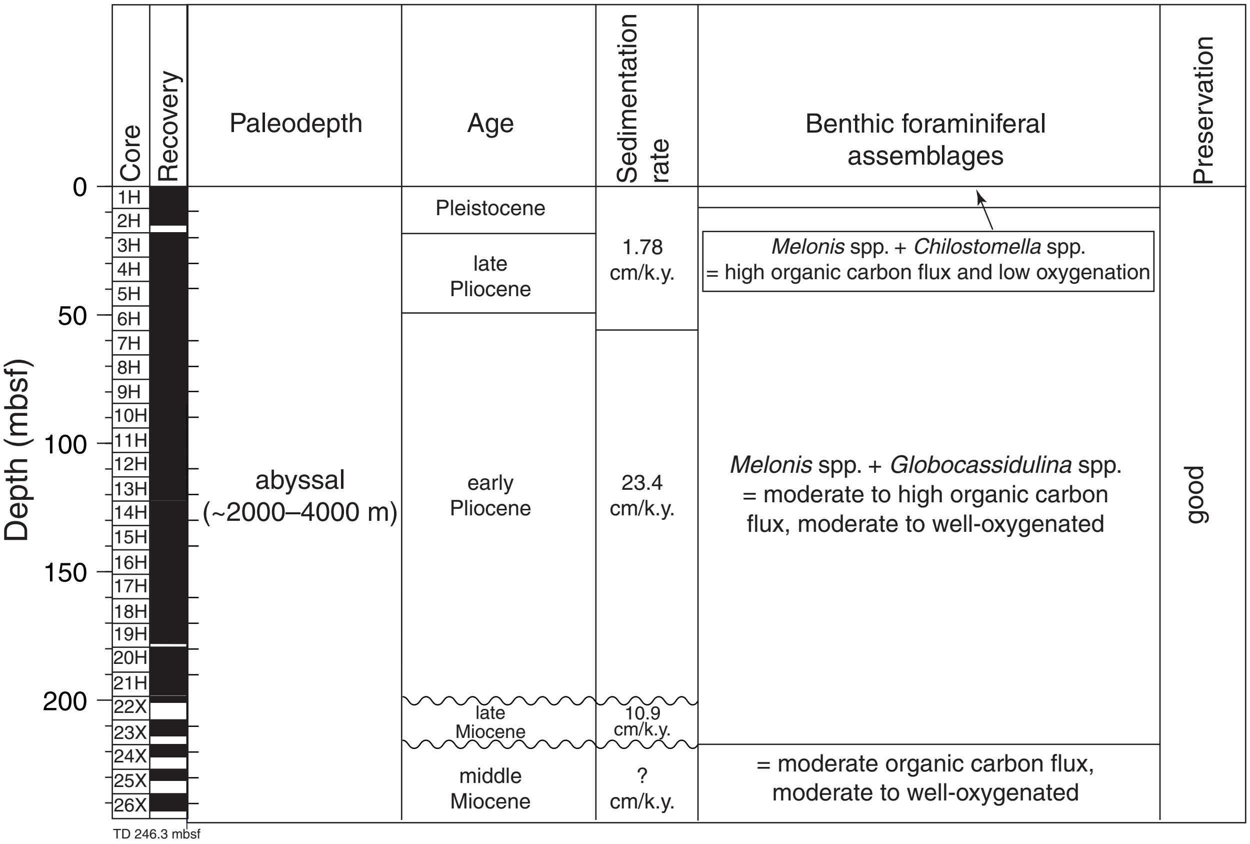

Figure F7. Long-core results showing limited magnetostratigraphy for the late Pliocene and early Pleistocene with boundaries in undisturbed core.

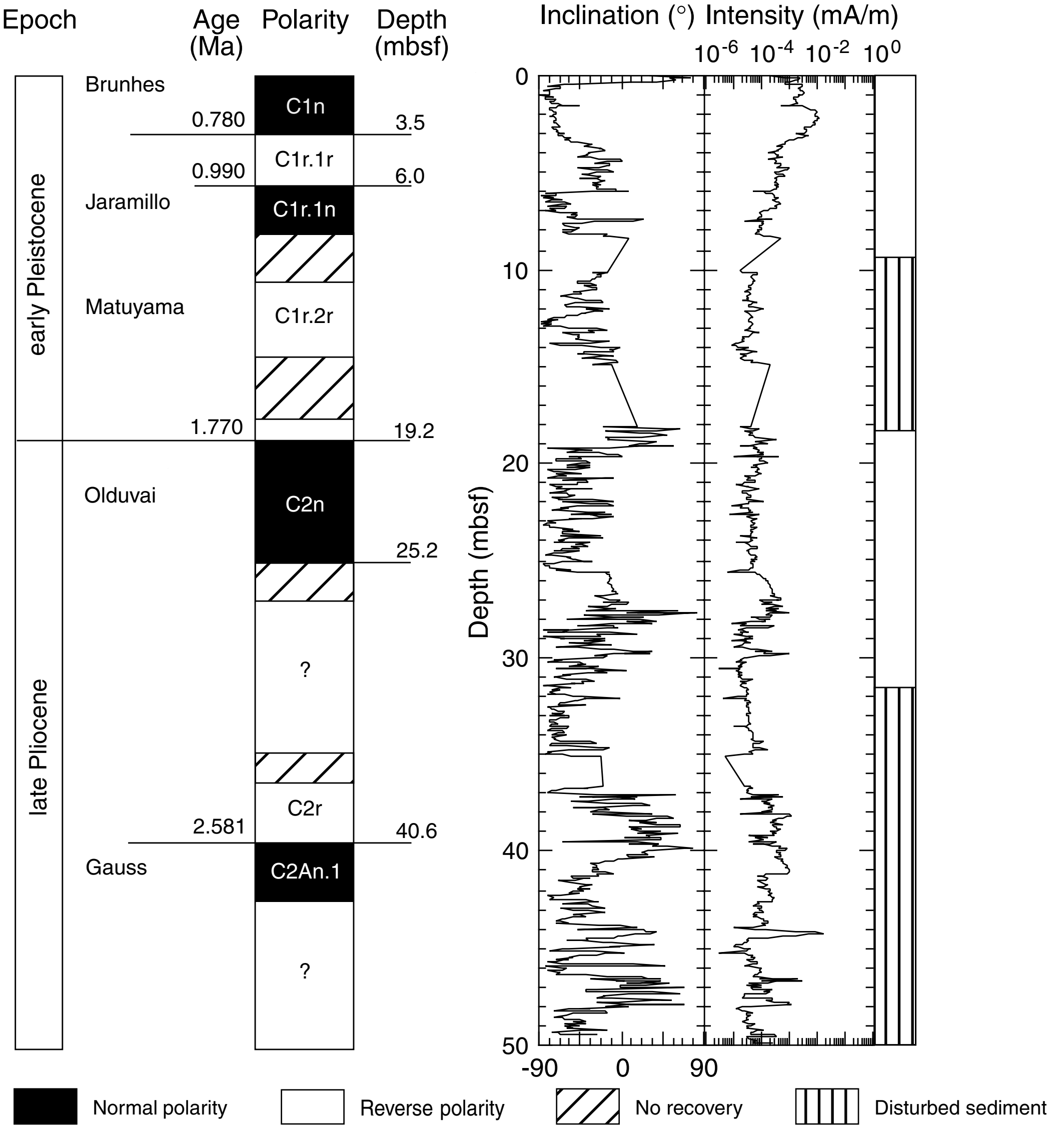

Figure F8. Magnetic characteristics for Sample 189-1169A-15H-6, 77–79 cm, and for Sample 22X-1, 50–52 cm. The latter sample bears microtektite.

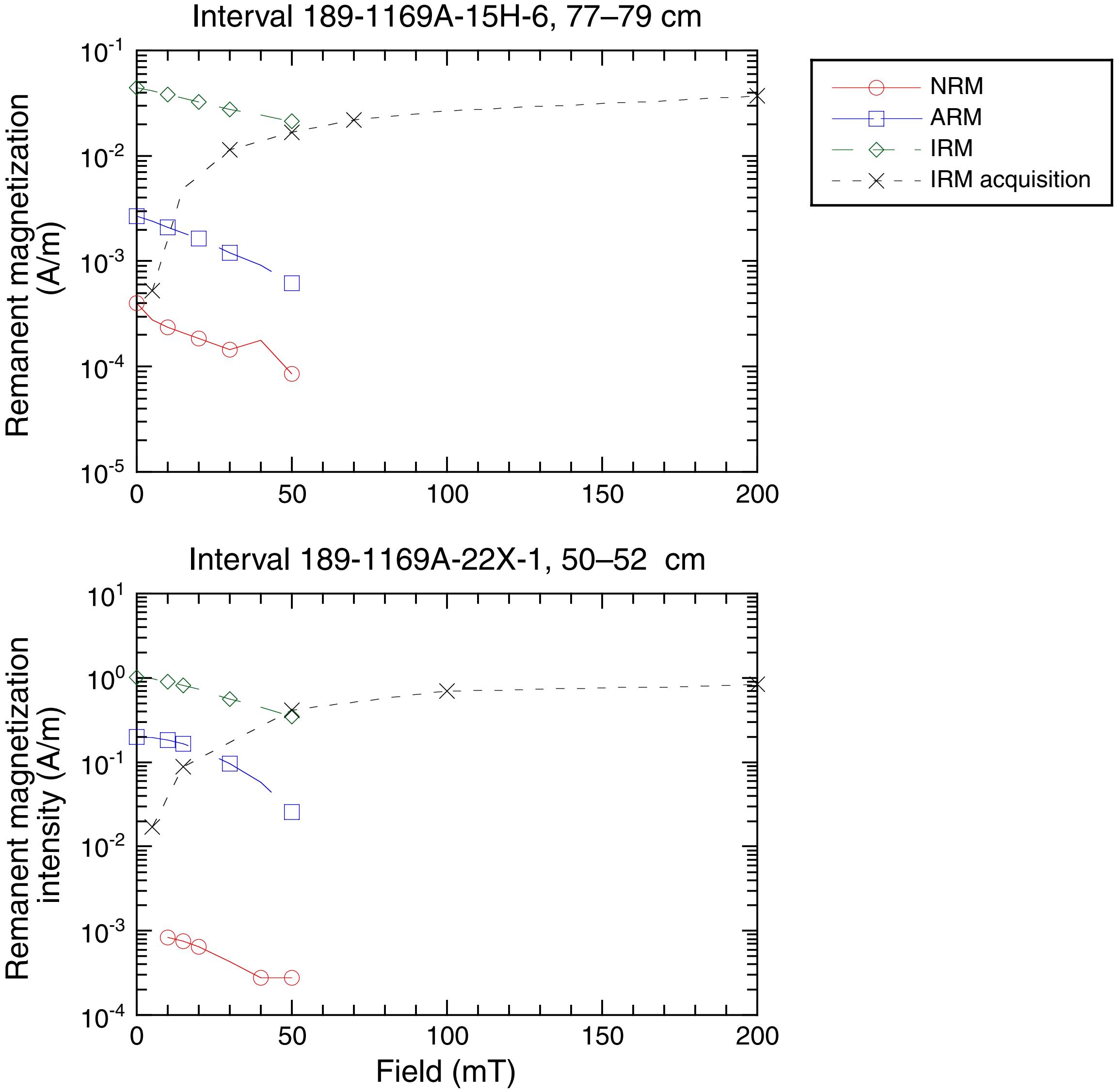

Figure F9. Plots of carbonate, total organic carbon (TOC), total nitrogen, and C/N ratios for Hole 1169A. Shaded areas on the C/N ratio plot delineate typical marine and terrestrial organic matter fields. Lithostratigraphic units are indicated on the far right side of the figure.

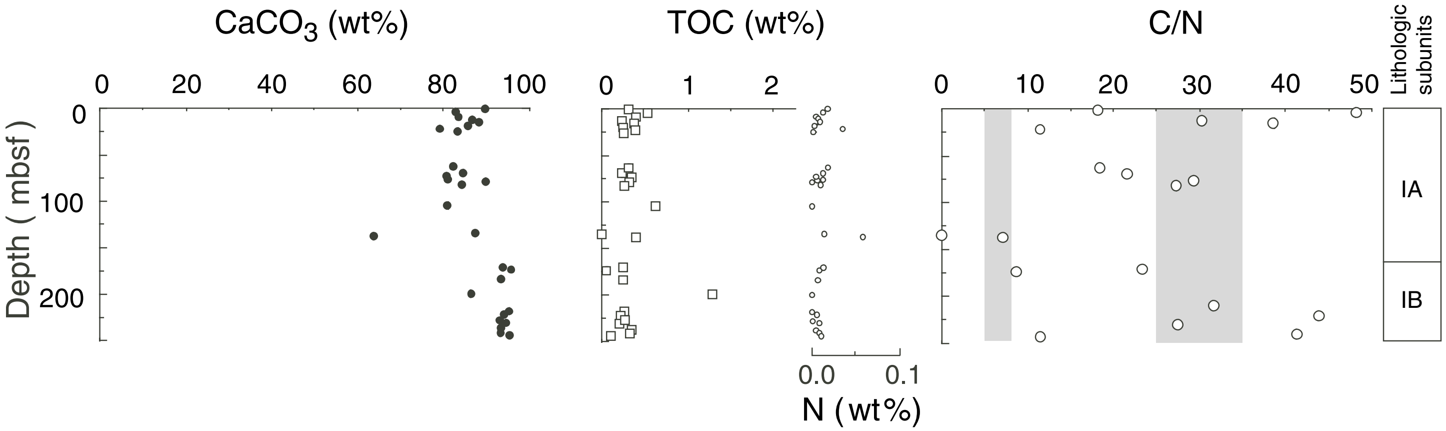

Figure F10. Concentration-depth profiles of Cl^- and Na^+ at Site 1169 with approximate location of lithostratigraphic boundaries (see **"Lithostratigraphy,"** p. 6). Standard seawater (SW) concentrations are indicated.

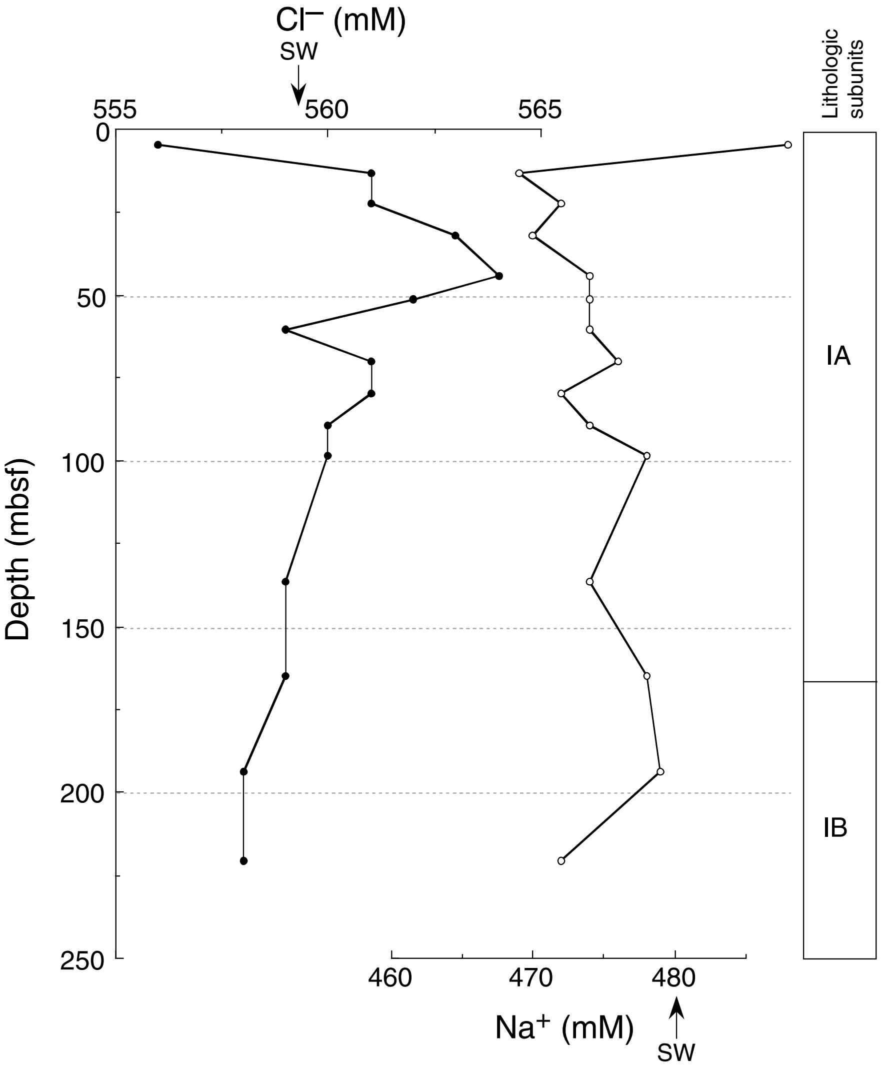

Figure F11. Concentration-depth profiles of SO_4^{2-}, pH, and alkalinity at Site 1169 with the approximate location of lithostratigraphic boundaries (see **"Lithostratigraphy,"** p. 6). Where appropriate, standard seawater (SW) concentrations are indicated.

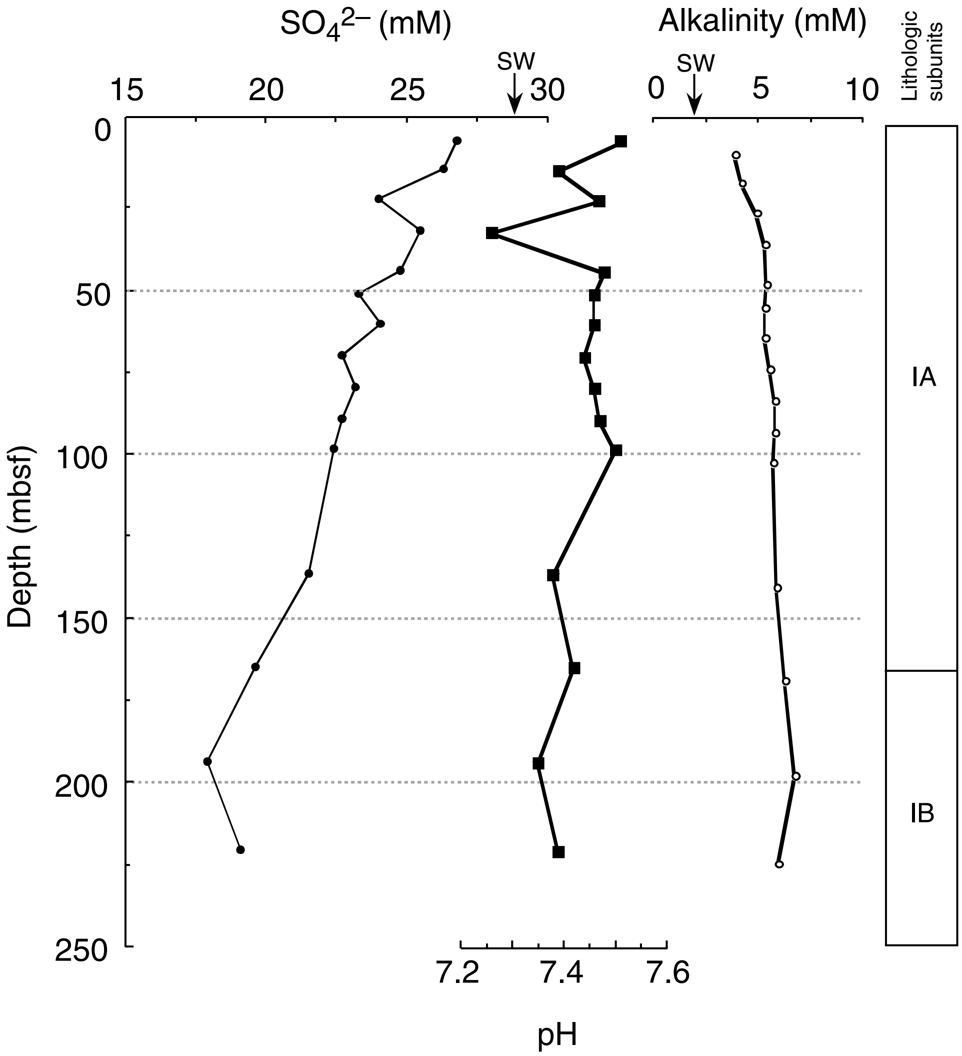

Figure F12. Concentration-depth profiles of Sr^{2+}, Ca^{2+}, and Li^{+} at Site 1169 with approximate location of lithostratigraphic boundaries (see **"Lithostratigraphy,"** p. 6). Standard seawater (SW) concentrations are indicated.

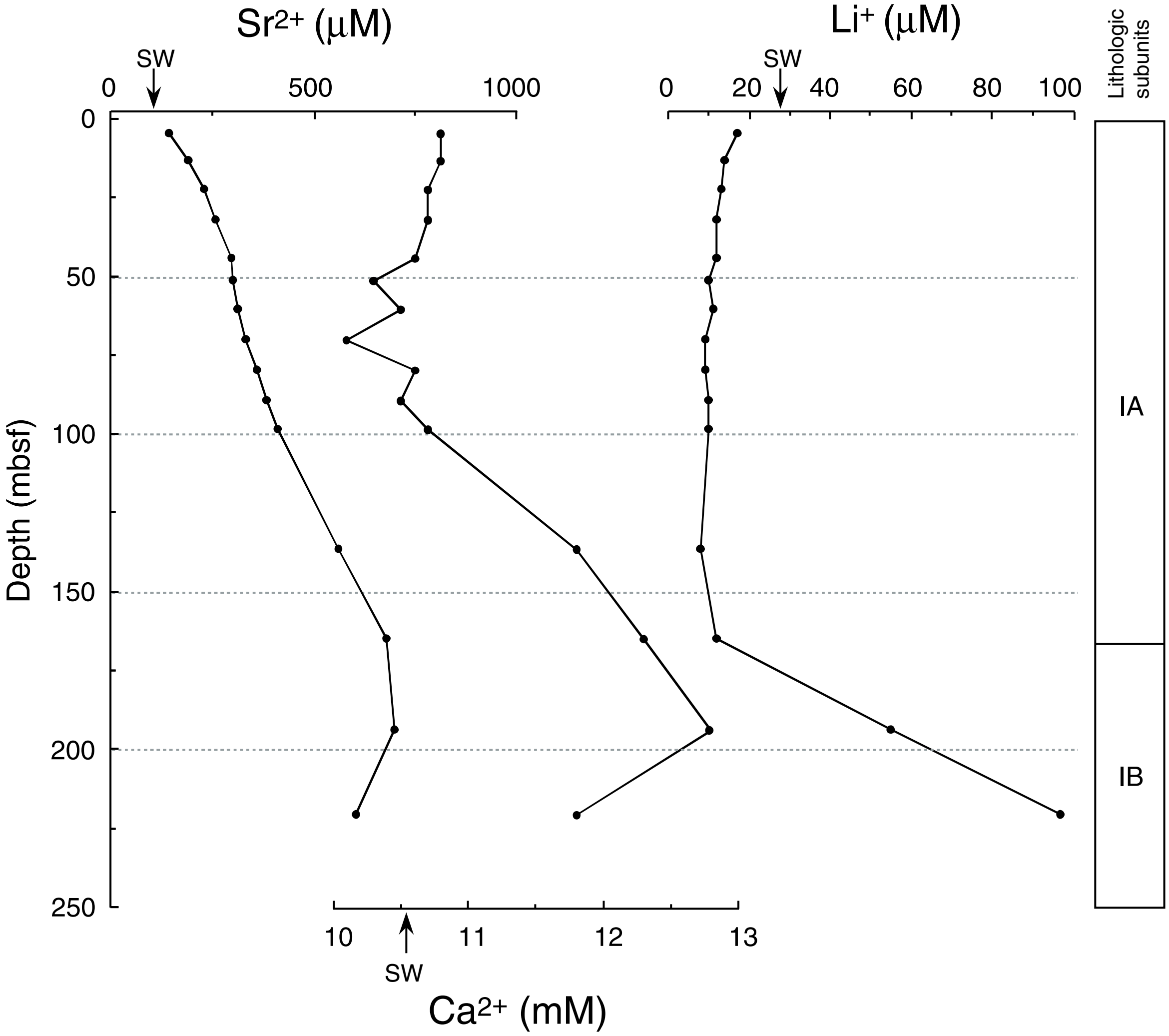

Figure F13. Concentration-depth profiles of Mg^{2+} and K^+ at Site 1169 with approximate location of lithostratigraphic boundaries (see **"Lithostratigraphy,"** p. 6). Standard seawater concentrations (SW) are indicated.

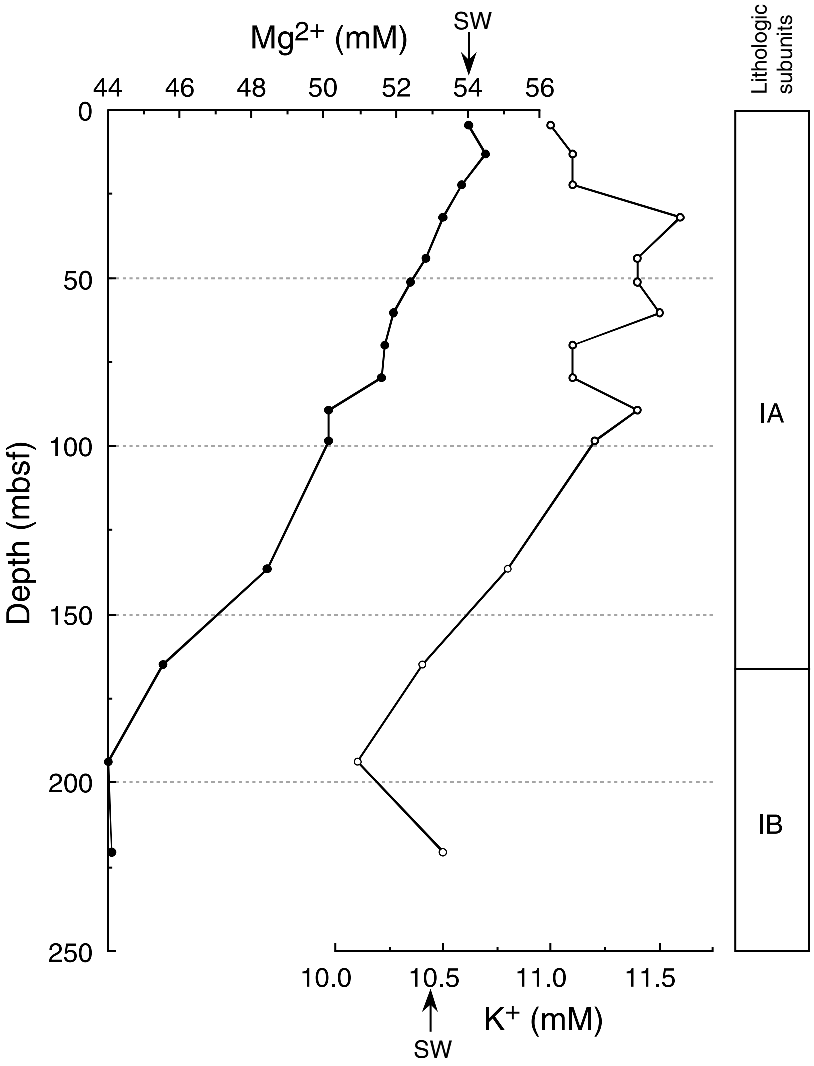

Figure F14. Concentration-depth profile of dissolved silica within interstitial water at Site 1169. Lithostratigraphic boundaries are indicated (see **"Lithostratigraphy,"** p. 6).

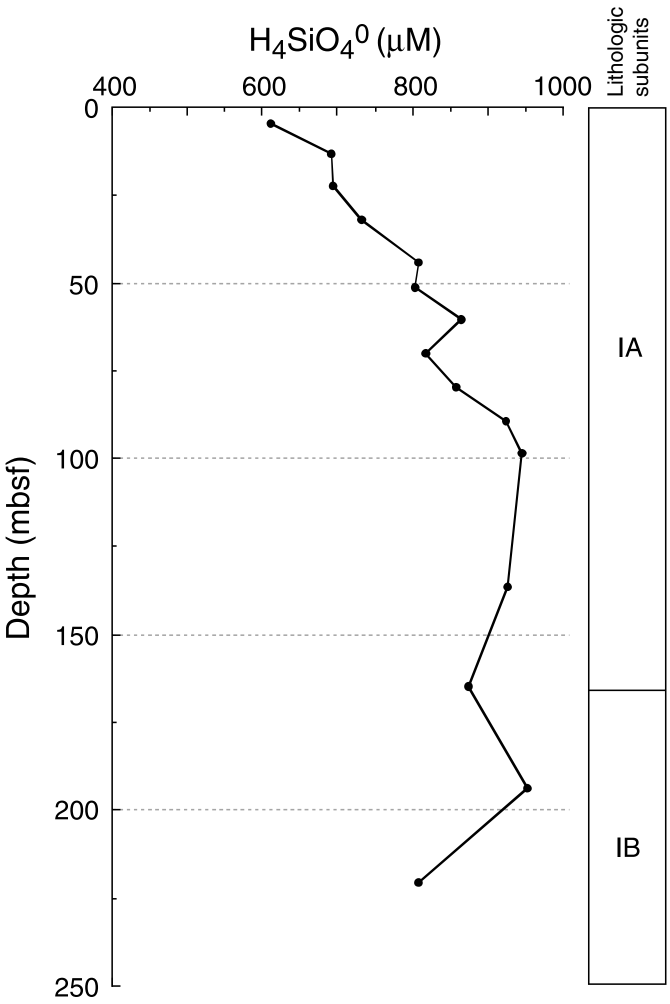

Figure F15. A. Magnetic susceptibility measured on whole cores by the MST vs. depth for Hole 1169A. There is little downcore variation in the magnetic susceptibility record, resulting from the high carbonate content of the sediments and the influence of flow-in. (Continued on next page.)

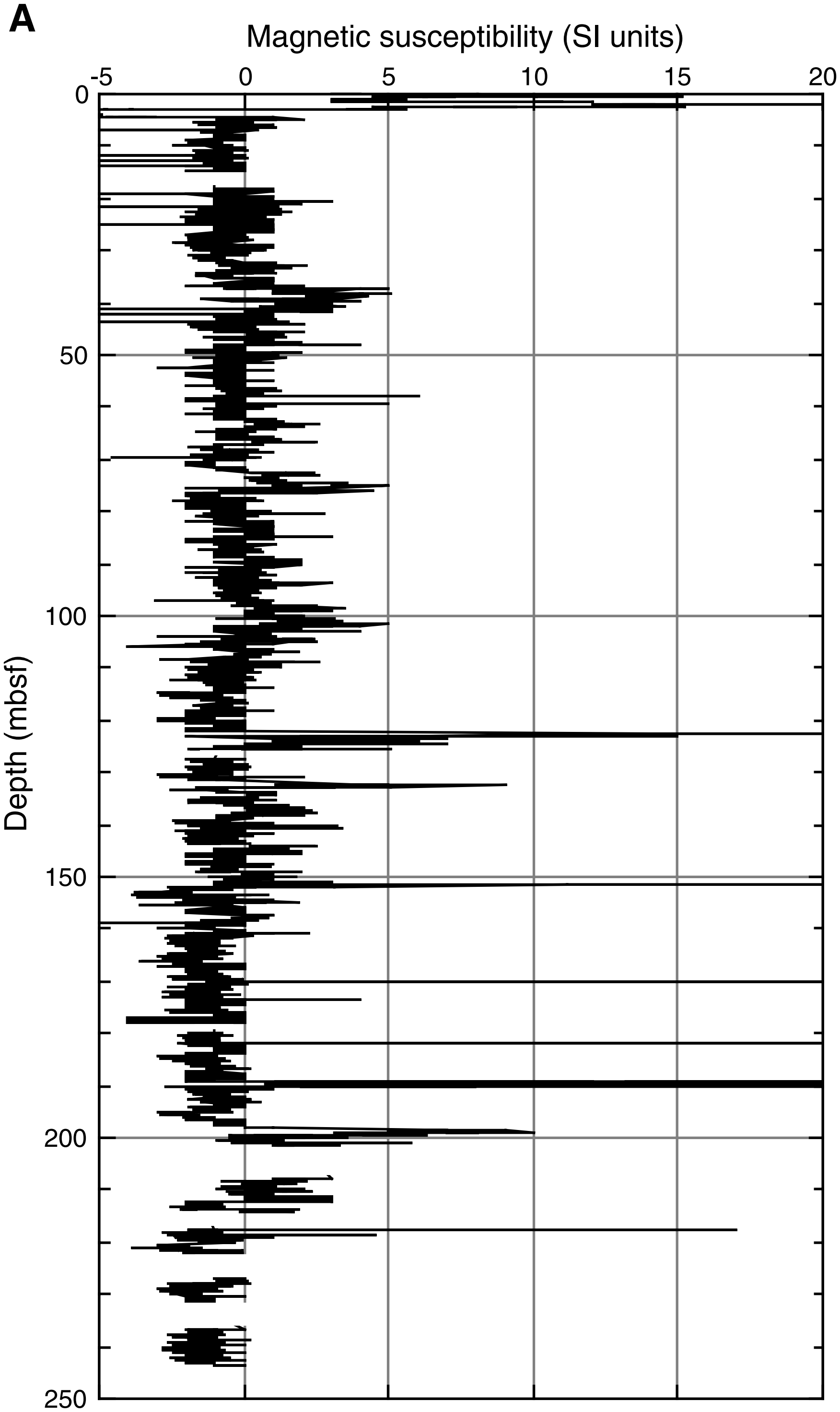

Figure F15 (continued). B. GRA density (open circles) and wet bulk density determined for discrete samples (solid diamonds) vs. depth for Hole 1169A. The two techniques provide similar data; however, because of the presence of flow-in and the high degree of disturbance in the cores, variation may be caused by the disturbance rather than lithologic change.

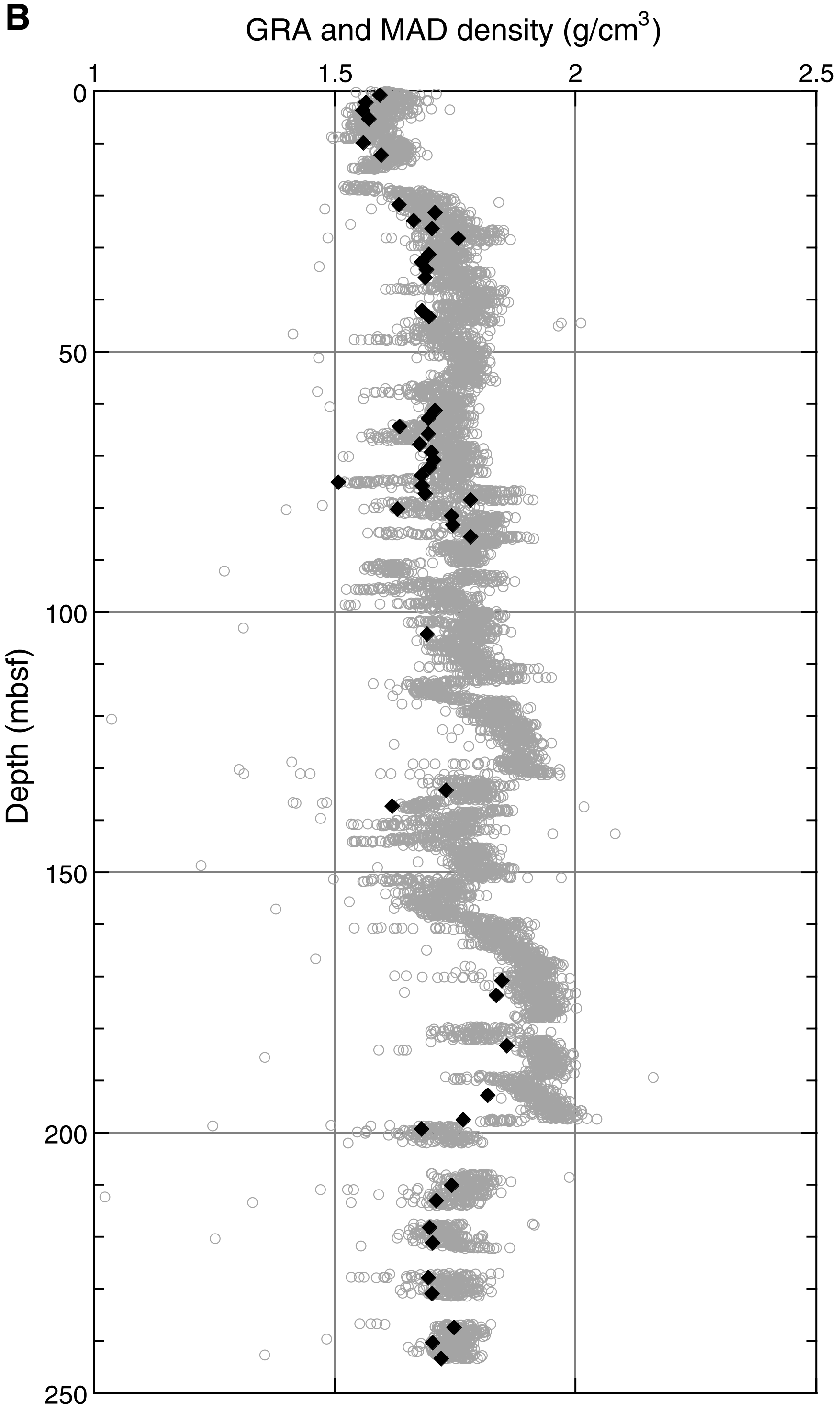

Figure F16. *P*-wave velocities (PWS1, PWS2, and PWS3) measured for discrete samples and *P*-wave velocities measured in whole cores (MST) vs. depth for Site 1169.

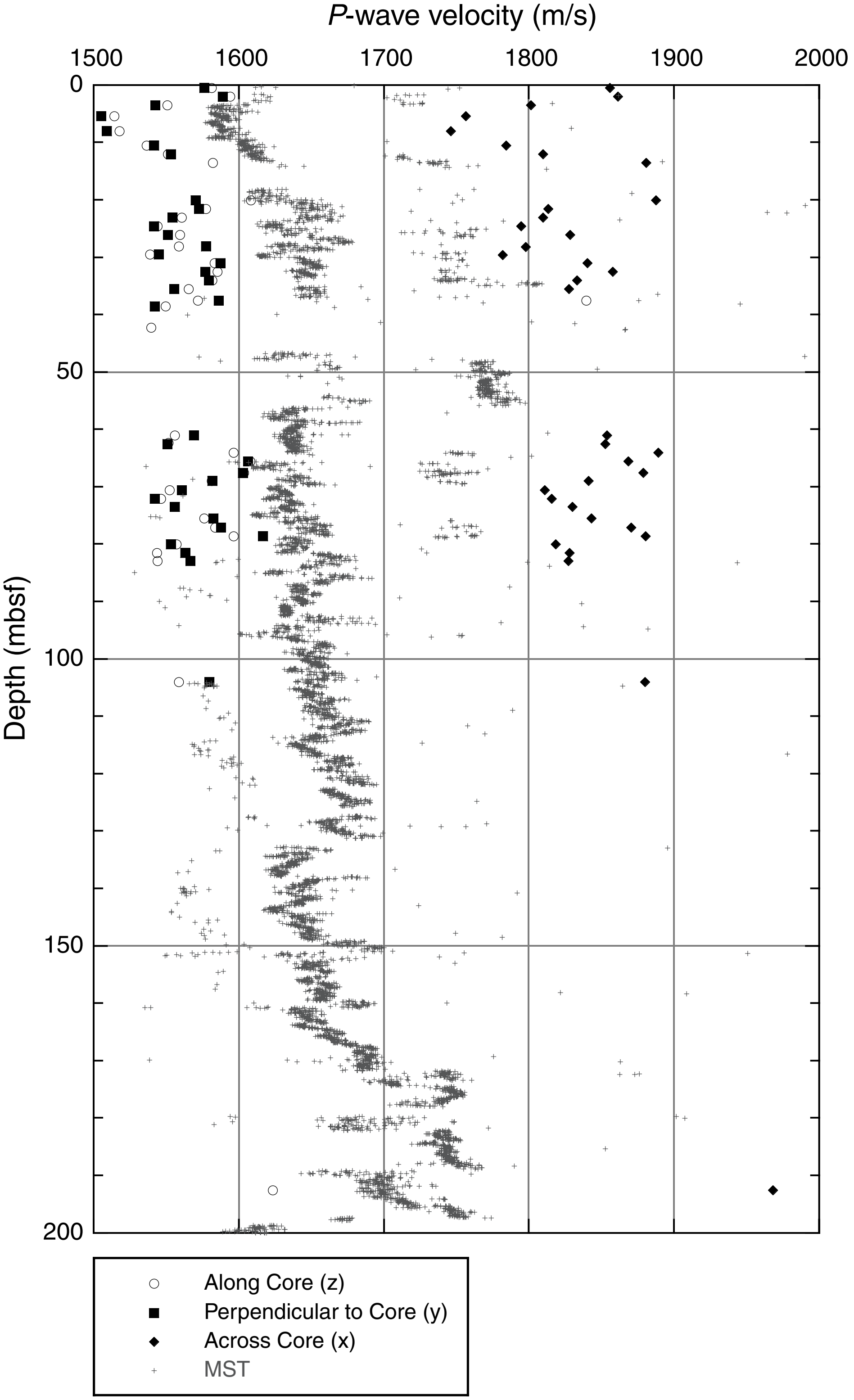

Figure F17. Shear strength measured on whole cores vs. depth, Hole 1169A. Interpretation of shear strength data is limited by the presence of flow-in and the high degree of disturbance in most cores.

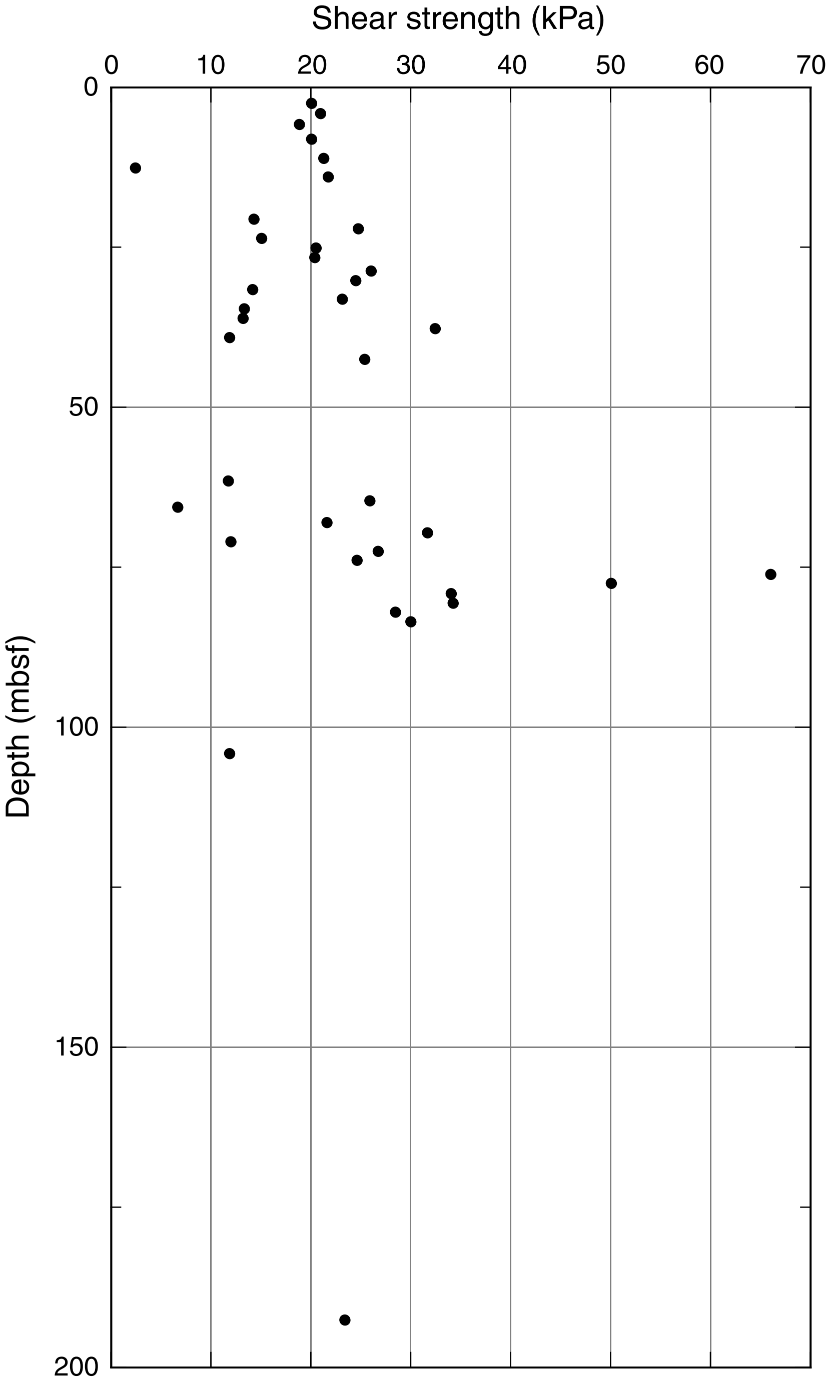

Figure F18. Thermal conductivity measured on whole cores vs. depth, Hole 1169A.

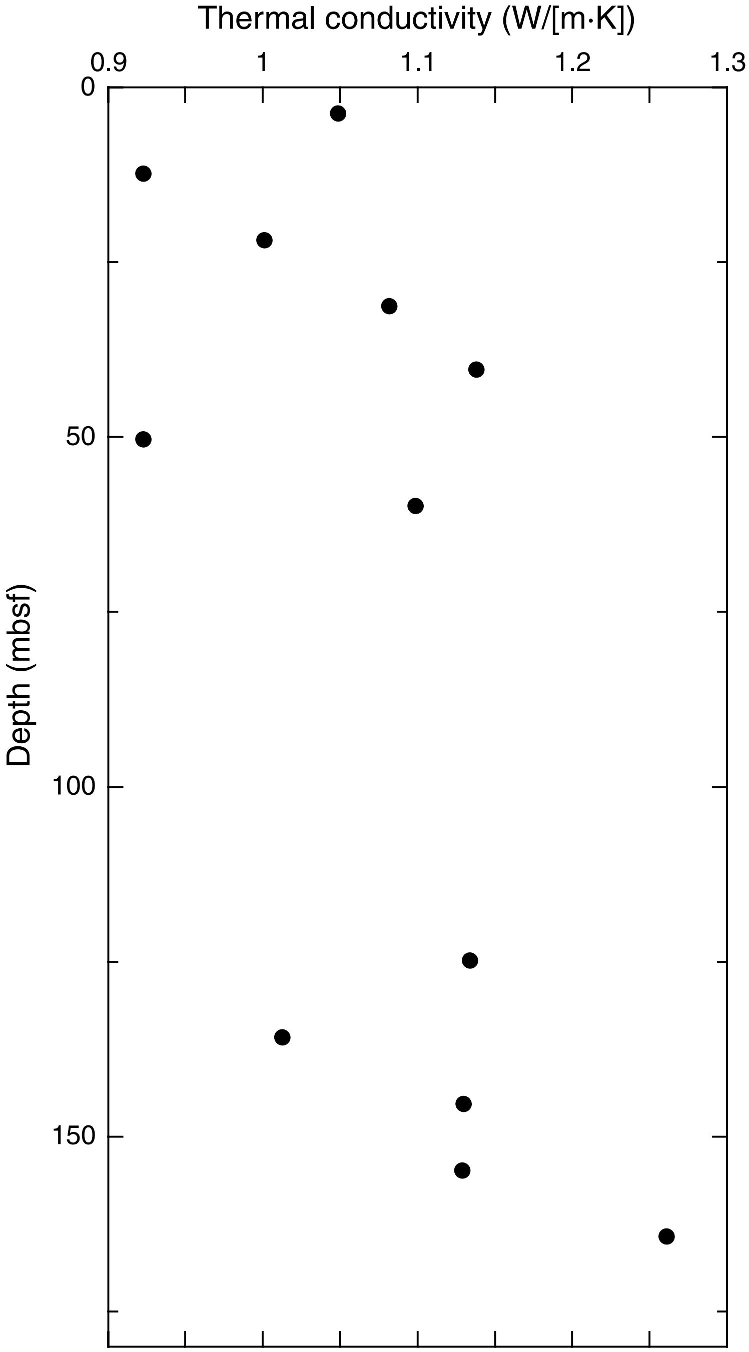

Figure F19. Wet bulk density, water content, and porosity measured at discrete intervals vs. depth for Hole 1169A. Discrete wet bulk density correlates well to GRA density (Fig. **F15B,** p. 43). However, interpretation of all downcore trends in physical properties is difficult because of the influence of flow-in and highly disturbed sediments.

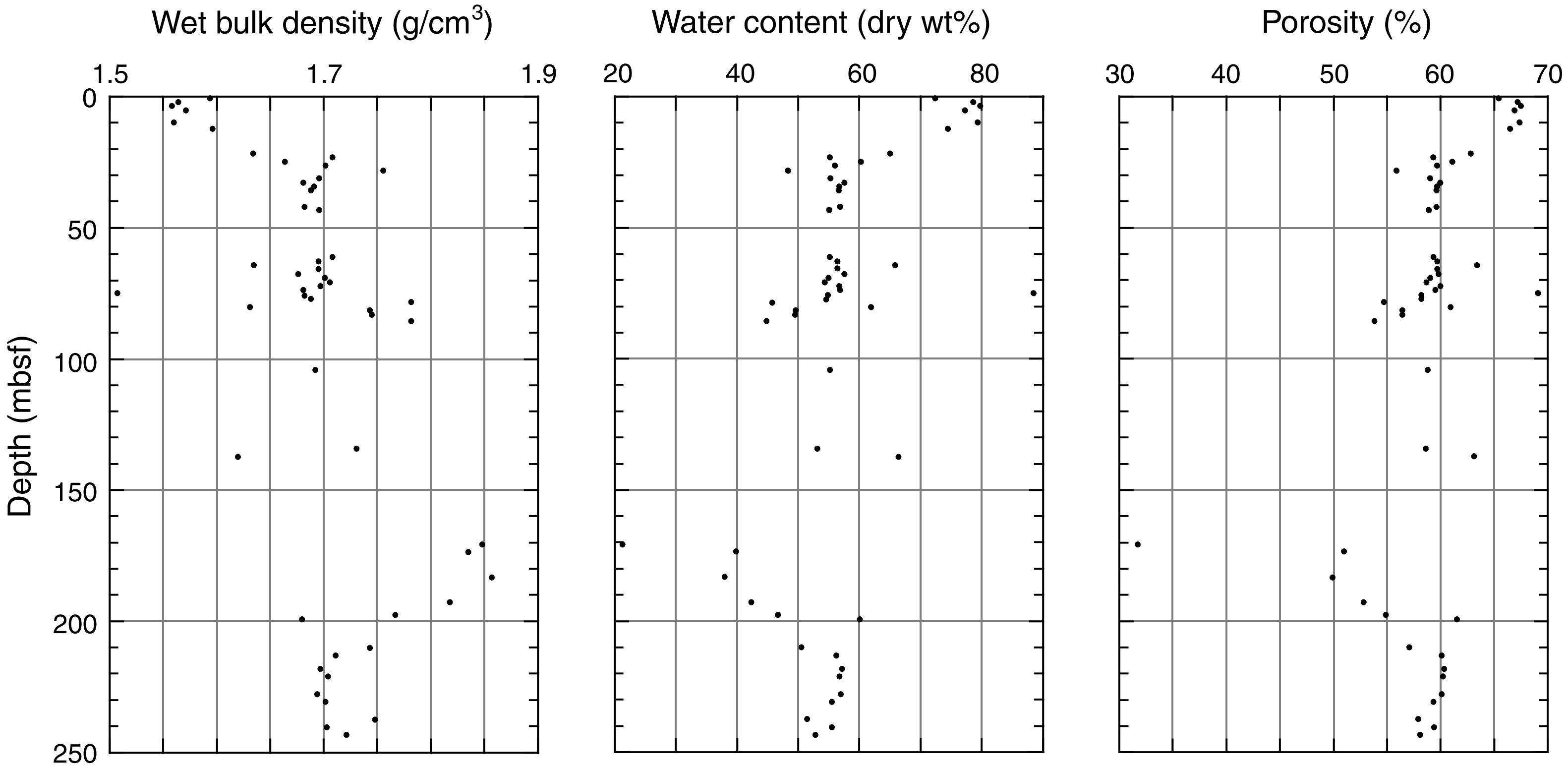

Table T1. Coring summary, Site 1169.

Hole 1169A
Latitude: 47°3.9159′S
Longitude: 145°14.2089′E
Time on site: 2 days, 19 hr, 45 min; 67.75 hr (1245 hr, 28 March–0830 hr, 31 March 2000)
Time on hole: 2 days, 19 hr, 45 min; 67.75 hr (1245 hr, 28 March–0830 hr, 31 March 2000)
Seafloor (drill pipe measurement from rig floor, mbrf): 3578.9
Distance between rig floor and sea level (m): 11.0
Water depth (drill pipe measurement from sea level, m): 3567.9
Total depth (from rig floor, mbrf): 3825.2
Total penetration (mbsf): 246.3
Total length of cored section (m): 246.3
Total core recovered (m): 225.02
Core recovery (%): 91.4
Total number of cores: 26

Core	Date (March 2000)	Time (local)	Depth (mbsf)		Length (m)		Recovery (%)
			Top	Bottom	Cored	Recovered	
189-1169A-							
1H	28	2320	0.0	8.6	8.6	8.56	99.5
2H	29	0025	8.6	18.1	9.5	6.49	68.3
3H	29	0125	18.1	27.6	9.5	9.85	103.7
4H	29	0225	27.6	37.1	9.5	9.80	103.2
5H	29	0520	37.1	46.6	9.5	9.74	102.5
6H	29	0640	46.6	56.1	9.5	9.56	100.6
7H	29	0720	56.1	65.6	9.5	9.95	104.7
8H	29	0850	65.6	75.1	9.5	9.77	102.8
9H	29	1040	75.1	84.6	9.5	9.36	98.5
10H	29	1200	84.6	94.1	9.5	9.95	104.7
11H	29	1310	94.1	103.6	9.5	10.05	105.8
12H	29	1420	103.6	113.1	9.5	9.94	104.6
13H	29	1630	113.1	122.6	9.5	9.25	97.4
14H	29	2010	122.6	132.1	9.5	9.61	101.2
15H	29	2325	132.1	141.6	9.5	10.04	105.7
16H	30	0100	141.6	151.1	9.5	9.91	104.3
17H	30	0230	151.1	160.6	9.5	10.00	105.3
18H	30	0815	160.6	170.1	9.5	9.82	103.4
19H	30	1005	170.1	179.6	9.5	8.11	85.4
20H	30	1230	179.6	189.1	9.5	9.78	103.0
21H	30	1520	189.1	198.6	9.5	9.14	96.2
22X	30	1755	198.6	207.9	9.3	3.51	37.7
23X	30	1940	207.9	217.5	9.6	6.34	66.0
24X	30	2115	217.5	227.1	9.6	4.88	50.8
25X	30	2245	227.1	236.7	9.6	4.53	47.2
26X	31	0015	236.7	246.3	9.6	7.08	73.8
				Totals:	246.3	225.02	91.4

Table T2. Distribution and abundances of nannofossils, Hole 1169A.

Core, section, interval (cm)	Depth (mbsf)	Preservation	Group abundance	*Amaurolithus delicatus*	*Amaurolithus primus*	*Calcidiscus leptoporus*	*Calcidiscus macintyrei*	*Calcidiscus premacintyrei*	*Ceratolithus armatus*	*Ceratolithus rugosus*	*Coccolithus miopelagicus*	*Coccolithus pelagicus*	*Cyclicargolithus floridanus*	*Dictyococcites productus*	*Discoaster bollii*	*Discoaster braarudii*	*Discoaster brouweri*	*Discoaster challengeri*	*Discoaster loeblichii*	*Discoaster surculus*	*Discoaster tamalis*	*Discoaster variabilis*	*Gephyrocapsa* spp. (small)	*Helicosphaera kamptneri*	*Helicosphaera sellii*	*Pseudoemiliania lacunosa*	*Reticulofenestra minuta*	*Reticulofenestra perplexa*	*Reticulofenestra pseudoumbilicus*
189-1169A-																													
1H-CC, 17-21	8.52	G	A																				A			F			R
2H-CC, 12-17	15.04	G	A			A	F					A											R		R	A			
3H-CC, 15-20	27.90	M	A			A	A					A					R			R				R				R	
4H-CC, 10-15	37.35	G	A			A	A					A												F				R	F
5H-CC, 11-16	46.79	G	A		F	A	F			R		A								R					R				
6H-CC, 14-19	56.11	G	A			A	C		R			A						R						C					
7H-CC, 14-19	66.00	M	A			A	C					A								R				F					
8H-CC, 0-5	75.32	M	A				F			R		A																F	C
9H-CC, 9-14	84.41	M	A		R	A	F			R		A						R											
10H-CC, 22-27	94.50	M	A			A	F					A																	
11H-CC, 21-26	104.10	P	A			A	F					A																	
12H-CC, 23-27	113.50	M	A				F													R									
13H-CC, 20-25	122.30	M	A				F										R			R	R								
14H-CC, 73-78	132.16	M	A				F					A		A						R									
15H-CC, 20-25	142.09	G	A				C					C								R									
16H-CC, 13-18	151.46	G	A			A	C					A																	
17H-CC, 11-16	161.05	G	A			A	C					A								R					R				
18H-CC, 13-18	170.37	M	A		R	A	C			R		A					R			R					R				F
19H-CC, 8-13	178.16	M	A	R		A	C					A																	C
20H-CC, 23-29	189.32	M	A	R			C										R												C
21H-CC, 21-26	198.19	M	A				C										R												
22X-CC, 0-5	202.06	M	A				C					A		A															C
23X-3, 44-44	211.34	M	A				A					A																	C
23X-4, 25-25	212.65	M	A				A					A							F			C							F
23X-CC, 12-17	214.19	M	A	R			C					A		A															C
24X-1, 120-120	218.70	M	A					C											F			F							
24X-2, 60-60	219.60	M	A					C			C				R	R						C							
24X-3, 10-10	220.60	M	A				A	C			C											F							
24X-4, 35-35	222.05	M	A										C																
24X-CC, 8-13	222.33	M	A				C	R					C																
25X-CC, 14-19	231.58	M	A				C																				A		C
26X-CC, 21-26	243.73	M	A				C	R					A									R						C	

Notes: Abundance: A = abundant, C = common, F = few, R = rare. Preservation: G = good, M = moderate, P = poor.

Table T3. Calcareous nannofossil datum levels and their assigned age estimates, Hole 1169A.

Datum	Age (Ma)	Interval (cm)		Depth (mbsf)		Mean (m)	Error bar (m)	References
		Top	Bottom	Top	Bottom			
LO *Reticulofenestra pseudoumbilica*	3.65	3H-CC	4H-CC	27.90	37.35	32.63	4.73	Berggren et al., 1995
LO *Amaurolithus primus*	4.60	5H-CC	6H-CC	46.79	56.11	51.45	4.66	Berggren et al., 1995
LO *Discoaster loeblechii*	6.80	23X-3, 44	23X-4, 25	211.34	212.65	212.00	0.66	Berggren et al., 1995
LO *Amaurolithus delicatus*	6.90	23X-CC	24X-1, 120	214.19	215.39	214.79	0.60	Gartner, 1992
FO *Discoaster loeblechii*	8.70	24X-1, 120	24X-2, 60	218.70	219.60	219.15	0.45	Berggren et al., 1995
LO *Cyclicargolithus floridanus*	11.90	24-3, 10	24-4, 35	220.60	222.05	221.33	0.73	Gartner, 1992

Notes: The depth of each datum is assigned at the midpoint between depths of observed samples. LO = last occurrence, FO = first occurrence.

Table T4. Range chart of planktonic foraminifers, Hole 1169A.

Hole, core, section	Depth (mbsf)	*Beella digitata*	*Globigerina bulloides*	*Globigerina falconensis*	*Globigerina praebulloides*	*Globigerina quinqueloba*	*Globigerinella aequilateralis*	*Globigerinella obesa*	*Globigerinita glutinata*	*Globigerinita naparimaensis*	*Globigerinita uvula*	*Globorotalia crassaconica*	*Globorotalia crassaformis* (sin)	*Globorotalia crassula*	*Globorotalia fohsi lobata*	*Globorotalia hirsuta*	*Globorotalia inflata* (sin)	*Globorotalia panda*	*Globorotalia pliozea*	*Globorotalia puncticulata*	*Globorotalia puncticuloides*	*Globorotalia scitula*	*Globorotalia sphericomiozea*	*Globorotalia triangula*	*Globorotalia truncatulinoides*	*Globoturborotalita apertura*	*Globoturborotalita decoraperta*	*Neogloboquadrina continuosa*	*Neogloboquadrina dutertrei*	*Neogloboquadrina pachyderma* (sin)	*Orbulina universa*	*Paragloborotalia continuosa*	*Paragloborotalia mayeri*	*Paragloborotalia nympha*	Zone/ Subzone	Age	
189-1169A-																																					
1H-CC	8.52		X			X			X		X		X	X			X							X	X					X	X				SN14	Pleistocene	
2H-CC	15.04	X	X	X		X	X	X	X		X	X	X	X							X	X		X	X				X	X	X				SN12b	late	Plio.
3H-CC	27.90		X			X			X	X	X		X	X						X	X										X						
4H-CC	37.35		X	X			X	X	X		X	X	X							X	X	X	?			X				X	X						
5H-CC	46.79		X	X		X			X				X						?	X	X									X	X						
6H-CC	56.11		X	X		X			X				X						?	X	X	X								X	X						
7H-CC	66.00		X	X		X			X				X			X	X			X		X								X	X						
8H-CC	75.32		X	X		X			X								X			X	X									X	X						
9H-CC	84.41		X	X		X			X											X	X	X								X	X						
10H-CC	94.50		X	X		X											X			X	X	X	?							X	X						
11H-CC	104.10		X	X		X											X			X	X		?							X							
12H-CC	113.50		X	X		X			X				X	X						X	X									X							
13H-CC	122.30		X	X		X			X				X	X						X	X									X	X						
14H-CC	132.16		X	X		X							X		X					X	X										X						
15H-CC	142.09		X	X		X														X	X	X	?							X							
16H-CC	151.46		X	X		X			X				X	X			?			X	X	X	?							X							
17H-CC	161.05		X	X		X			X				X	X						X	X																
18H-CC	170.37		X			X			X				X				?			X	X	X	?							X	X						
19H-CC	178.16		X	X		X			X				X							X	X	X	?							X	X						
20H-CC	189.32		X	X		X							X							X	X									X	X						
21H-CC	198.19		X			X							X							X	X		?							X	X						
22H-CC	202.06		X			X		X									X	?	X	X	X						X				X				SN12a	early	
23H-CC	214.19				X	X														X											X	X	X	X	SN7	middle	Miocene
24H-CC	222.33		X			X			X		X						X		X	X	X							X									
25H-CC	231.58		X			X			X								X			X	X			X	X					X							
26H-CC	243.73		X						X												X														SN1	early	

Note: X = present, ? = questionable identification.

Table T5. Planktonic foraminifer datum levels, Hole 1169A.

Bioevent	Age (Ma)	Interval		Depth (mbsf)		Mean (mbsf)	Error bar (m)
		Top	Bottom	Top	Bottom		
LO *Globorotalia pliozea*	4.60	21H-CC	22H-CC	198.18	202.06	200.120	1.940
LO *Paragloborotalia mayeri*	11.40	22X-CC	23X-CC	202.06	214.19	208.125	6.065

Note: LO = last occurrence.

Table T6. Relative abundance of selected diatom taxa, sponge spicules, and silicoflagellates, Hole 1169A.

Core, section, interval (cm)	Depth (mbsf)	Group preservation	Group abundance	*Actinocyclus curvatulus*	*Actinocyclus fryxellae*	*Actinocyclus ingens*	*Actinocyclus ingens* var. *nodus*	*Actinocyclus ingens* var. *ovalis*	*Asteromphalus* spp.	*Azpeitia nodulifer*	cf. *Azpeitia nodulifer*	*Azpeitia tabularis group*	*Cestodiscus antarcticus*	*Chaetoceros* resting spores	*Coscinodiscus marginatus*	*Coscinodiscus rhombicus*	*Denticulopsis dimorpha*	*Denticulopsis hustedtii*	*Diploneis bombus*	*Ethmodiscus rex*	*Eucampia antarctica*	*Fragilariopsis barronii*	*Fragilariopsis fossilis*	*Fragilariopsis kerguelensis*	*Fragilariopsis lacrima*	*Fragilariopsis reinholdii*	*Fragilariopsis ritscheri*	*Fragilariopsis* spp.	*Fragilariopsis weaveri*	*Hemidiscus* cf. *cuneiformis*	*Hemidiscus cuneiformis*	*Hemidiscus karstenii*	*Lisitzinia ornata*	*Nitzschia donahuensis*	*Proboscia barboi*	*Rhizosolenia* spp.	*Rocella gelida*	*Rocella gelida* var. *schraderi*	Silicoflagellate tests	Sponge spicules	*Synedra jouseana*	*Thalassionema nitzschioides*	*T. nitzschioides* var. *parva*	*Thalassiosira complicata*	*Thalassiosira convexa*	*Thalassiosira eccentrica*	*Thalassiosira elliptipora*	*Thalassiosira fasciculata*	*Thalassiosira gracilis*	*Thalassiosira insigna*	*Thalassiosira inura*	*Thalassiosira lentiginosa*	*Thalassiosira leptopus*	*Thalassiosira oestrupii*	*Thalassiosira oliverana*	*Thalassiosira* spp.	*Thalassiosira torokina*	*Thalassiosira striata*	*Thalassiosira symmetrica*	*T. tetraoestrupii* var. *reimeri*	*Thalassiosira torokina*	*Thalassiothrix antarctica*
189-1169A-																																																														
1H-CC, 17-21	8.52	MG	C			C				C		R			C				R		R			A		R	F				A	F			C				C	A						F						R	R		C							A
2H-CC, 12-17	15.04	G	C									R		R	F		R			P		C		C		R			C		C	C			A				C	A		R				F				F	F			F	F	F						A
3H-CC, 15-20	27.90	G	C			R				R				R						P						C			C		C	F			F				F	A		R		R		R				F	F		R	R	C	R						D
4H-CC, 10-15	37.35	P	A		F	C			R	R		R			R					P		F		F			R				F	R			C	R			F	A		R	R				R		R			C	R	R	F							D
5H-CC, 11-16	46.79	M	A							R					F					P		F			R						F				C				F	A						F				C					C				R			D
6H-CC, 14-19	56.11	MG	R			D									F					P		F	F									R							F	F		R				R							F	R	F							C
7H-CC, 14-19	66.00	M	C			F						R			R					P		F	C												C	R			F	C		F							R					F					R			C
8H-CC, 0-5	75.32	MG	A			R								R	C					P	R									D	A	F							F	A		R									R				F							C
9H-CC, 9-14	84.41	MG	C		R	C				R					P					P				R	R	F		R	C	R	F	F		R					F	C					F						F				C			R			R	C
10H-CC, 22-27	94.50	M	A			F									P					P	P	C	F		P	F			P		P			P	D				F	A		P				R							C	P	P							C
11H-CC, 21-26	104.10	G	C									P			C							C							P	P					C				P	C				P								P	F	F	F							C
12H-CC, 23-27	113.50	MG	A	P						F				P	P										P	P			C	P	P	C							P	C				F						P	P			P	C						P	D
13H-CC, 20-25	122.30	M	C			C								P						P									F			P							P	F								P							P							C
14H-CC, 73-78	132.16	P	T																																				P	R																						T
15H-CC, 20-25	142.09	G	C												F							C									C								P	C															F							C
16H-CC, 13-18	151.46	M	C			C									C					P		C									C								P	C															C							D
17H-CC, 11-16	161.05	G	C			C						P																	C			P							P	C								F							P		P					C
18H-CC, 13-18	170.37	P	R					T																																R																						R
19H-CC, 8-13	178.16	P	R								R															P									R					R																						R
20H-CC, 23-29	189.32	P	F		F	F				F					T					P			P								P	P			R																					P				P		F
21H-CC, 21-26	198.19	P	T																	P		R																																								T
22X-CC, 0-5	202.06	P	T		T	T																																		F																						T
23X-CC, 12-17	214.19	P	F			F											F	P																						F																						T
24X-CC, 8-13	222.33	MG	F			C	P										C																				F	C		C	F																					P
25X-CC, 14-19	231.58	P	F			F									F		C														P				R					F																						P
26X-CC, 21-26	243.73	P	T														T																																													T

Notes: Preservation: G = good, M = moderate, P = poor. Abundance: D = dominant, A = abundant, C = common, F = few, R = rare, T = trace, B = barren.

Table T7. Combined bioevents used for the age model, Hole 1169A.

Group	Bioevent	Age (Ma)	Interval (cm)		Depth (mbsf)
			Top	Bottom	
D	LO *Proboscia barboi*	1.80	0.0	1H-CC	8.52
R	LO *Pseudocubus vema*	2.40	4H-CC	5H-CC	42.07
C	LO *Invertocysta tabulata*	2.65	5H-CC	9H-CC	65.50
D	LO *Fragilariopsis weaveri*	2.65	1H-CC	2H-CC	15.04
D	LO *Fragilariopsis lacrima*	2.90	4H-CC	5H-CC	46.79
R	LO *Lampromitra coronata*	3.35	6H-CC	7H-CC	61.06
N	LO *Reticulofenestra pseudoumbilica*	3.65	3H-CC	4H-CC	32.63
N	LO *Amaurolithus primus*	4.60	5H-CC	6H-CC	51.45
F	LO *Globorotalia pliozea*	4.60	21H-CC	22H-CC	200.13
R	LO *Lychnocanoma grande*	5.00	16H-CC	17H-CC	156.30
R	LO *Dictyophimus splendens*	5.20	21H-CC	22X-CC	200.13
B	LO *Bolboforma aculeata*	5.30	21H-CC	22X-CC	200.13
D	LO *Actinocyclus fryxellae*	6.70	20H-CC	21H-CC	198.19
N	LO *Discoaster loeblechii*	6.80	23X-3, 44	23X-4, 25	212.00
N	LO *Amaurolithus delicatus*	6.90	23X-CC	24X-1, 120	214.76
D	LO *Denticulopsis dimorpha*	10.70	23X-CC	24X-CC	222.33
F	LO *Paragloborotalia mayeri*	11.40	22X-CC	23X-CC	208.13
N	LO *Cyclicargolithus floridanus*	11.90	24X-3, 10	24X-4, 35	221.33
R	LAO *Cyrtocapsella tetrapera*	12.50	23X-CC	24X-CC	218.30

Notes: Group: D = diatom, R = radiolarian, C = dinocyst, N = nannofossil, F = planktonic foraminifer, B = bolboforma. LO = last occurrence, LAO = last abundant occurrence. This table is also available in **ASCII format.**

Table T8. Distribution of organic walled dinoflagellate cysts (number of dinocysts specimens) and percentages of sporomorph and foraminifer linings in selected samples, Hole 1169A.

Core, section, interval (cm)	Depth (mbsf)	Group abundance	Dinocysts (%)	Sporomorphs (%)	Foraminifer linings (%)	*Bitectatodinium tepikiense*	*Brigantedinium* spp.	*Corrudinium harlandii*	*Dalella chathamense*	*Impagidinium pallidum*	*Impagidinium aculeatum*	*Impagidinium japonicum*	*Impagidinium paradoxum*	*Impagidinium patulum*	*Impagidinium sphaericum*	*Impagidinium strialatum*	*Invertocysta tabulata*	*Nematosphaeropsis labyrinthea*	*Operculodinium centrocarpum*	*Selenopemphix antarctica*	*Spiniferites mirabilis*	*Spiniferites ramosus*
189-1169A-																						
1H-CC, 17-21	8.52	A	81.6	6.3	12.1	6	22	2	6	7	27	5	30	9	2	4		74	4	4	16	9
4H-CC, 10-15	37.35	C	83.4	8.8	7.8	3	18	3	1	2	34		26	4	11			34	4	4	18	9
5H-CC, 11-16	46.79	C	96.0	2.0	2.0						53		78		1			12				1
9H-CC, 9-14	84.41	C	87.5	8.3	4.2			5		2	22		5	4	1		2					
12H-CC, 23-27	113.50	B																				
15H-CC, 20-25	142.09	B																				
16H-CC, 13-18	151.46	T	100.0	0	0						3		8	2			1	3				
17H-CC, 11-16	161.05	T	100.0	0	0						2		4									
19H-CC, 8-13	178.16	B																				
21H-CC, 21-26	198.19	B																				
23X-CC, 12-17	214.19	B																				
24X-CC, 8-13	222.33	B																				

Notes: Abundance refers to abundance of dinocysts: A = abundant, C = common, F = few, R = rare, T = trace, B = barren.

Table T9. Selected age-diagnostic dinocyst event, Hole 1169A.

Dinocyst Datum	Interval		Depth (mbsf)		Mean (mbsf)	Error (m)	Age (Ma)	Source
	Top	Bottom	Top	Bottom				
LO *Invertocysta tabulata*	5H-CC	9H-CC	46.79	84.41	65.60	18.81	2.65	Williams et al., 1998

Note: LO = last occurrence.

Table T10. Magnetostratigraphic results, Site 1169.

Chron	Age (Ma)	Depth (mbsf)
Onset C1n	0.78	3.50
Termination C1r.1n	0.99	6.00
Termination C2n	1.77	19.20
Termination C2An.1n	2.58	40.60

Table T11. Values for inorganic carbon, calcium carbonate, total carbon, total organic carbon, total nitrogen, and hydrogen in sediments, Hole 1169A.

Hole, core, section	Depth (mbsf)	IC (wt%)	$CaCO_3$ (wt%)	TC (wt%)	TOC (wt%)	N (wt%)	H (mg H/g)
189-1169A-							
1H-1	0.72	10.78	89.80	11.09	0.31	0.02	0.12
1H-3	3.72	9.91	82.55	10.44	0.53	0.01	0.15
1H-5	6.72	NA	NA	NA	NA	NA	NA
2H-1	9.32	10.00	83.28	10.40	0.40	0.00	0.17
2H-3	12.32	10.39	86.54	10.63	0.24	0.01	0.15
2H-5	14.82	10.58	88.09	10.96	0.39	0.01	0.12
3H-1	18.82	10.30	85.82	10.54	0.24	0.00	0.15
3H-3	21.82	9.47	78.88	9.87	0.40	0.04	0.21
3H-5	24.82	9.99	83.24	10.24	0.25	0.00	0.17
7H-5	62.83	9.89	82.35	10.20	0.31	0.02	0.18
8H-3	69.32	10.16	84.65	10.40	0.24	0.01	0.15
8H-5	72.32	9.69	80.74	10.05	0.36	0.00	0.18
9H-1	75.82	9.75	81.20	10.10	0.35	0.01	0.18
9H-3	78.52	10.79	89.89	11.11	0.32	0.00	0.08
9H-5	81.64	10.11	84.25	10.36	0.25	0.01	0.14
12H-1	104.25	9.73	81.07	10.37	0.64	0.00	0.15
15H-2	134.32	10.50	87.50	10.47	0.00	0.01	0.11
15H-4	137.32	7.66	63.78	8.08	0.42	0.06	0.34
19H-1	170.83	11.23	93.58	11.49	0.26	0.01	0.06
19H-3	173.59	11.47	95.54	11.53	0.06	0.01	0.06
20H-3	183.33	11.22	93.42	11.47	0.25	0.01	0.07
22X-1	199.33	10.34	86.09	11.63	1.29	0.00	0.04
24X-1	218.22	11.43	95.25	11.69	0.26	0.00	0.04
24X-3	221.22	11.29	94.05	11.51	0.22	0.01	0.05
25X-1	227.88	11.19	93.25	11.47	0.28	0.00	0.05
25X-3	230.91	11.33	94.36	11.52	0.19	0.01	0.04
26X-1	237.42	11.20	93.28	11.55	0.35	0.00	0.04
26X-3	240.42	11.20	93.30	11.53	0.33	0.01	0.05
26X-5	243.42	11.44	95.26	11.54	0.10	0.01	0.05

Notes: IC = inorganic carbon, $CaCO_3$ = calcium carbonate, TC = total carbon, TOC = total organic carbon. NA = not analyzed.

Table T12. Headspace gas composition, Hole 1169A.

Hole, core, section	Depth (mbsf)	C_1 (ppmv)
189-1169A-		
1H-4	4.50	3
2H-4	13.10	5
3H-4	22.60	3
4H-4	32.10	6
5H-6	43.94	5
7H-4	60.60	15
8H-4	70.10	11
9H-4	79.60	15
10H-4	89.10	22
11H-4	98.60	21
12H-4	108.10	24
13H-4	117.60	17
14H-2	124.10	28
15H-4	136.60	62
16H-4	146.10	52
17H-4	155.60	34
18H-4	165.10	43
19H-4	174.60	31
20H-4	184.10	60
21H-4	193.60	66
22X-2	200.10	80
23X-3	210.90	93
24X-3	220.50	97
25X-3	230.10	41
26X-4	241.20	92

Note: C_1 = methane, ppmv = parts per million by volume.

Table T13. Interstitial water data, Hole 1169A.

Core, section, interval (cm)	Depth (mbsf)	pH	Alkalinity (mM)	Salinity	Cl^- (mM)	SO_4^{2-} (mM)	Na^+ (mM)	Mg^{2+} (mM)	Ca^{2+} (mM)	K^+ (mM)	$H_4SiO_4^0$ (µM)	Sr^{2+} (µM)	Li^+ (µM)
189-1169A-													
1H-3, 145-150	4.45	7.51	3.98	35.0	556	26.8	488	54.0	10.8	11.0	610	141	17
2H-3, 145-150	13.05	7.39	4.24	35.0	561	26.3	469	54.5	10.8	11.1	691	191	14
3H-3, 145-150	22.55	7.47	4.98	35.0	561	24.0	472	53.8	10.7	11.1	693	228	13
4H-3, 145-150	32.05	7.26	5.35	35.0	563	25.5	470	53.3	10.7	11.6	732	255	12
5H-6, 140-150	45.19	7.48	5.45	35.0	564	24.8	474	52.8	10.6	11.4	809	297	12
6H-3, 145-150	51.05	7.46	5.37	35.0	562	23.3	474	52.4	10.3	11.4	803	299	10
7H-3, 145-150	60.55	7.46	5.39	35.0	559	24.1	474	51.9	10.5	11.5	864	313	11
8H-3, 145-150	73.05	7.44	5.61	35.0	561	22.7	476	51.7	10.1	11.1	817	331	9
9H-3, 145-150	79.55	7.46	5.84	34.0	561	23.2	472	51.6	10.6	11.1	858	360	9
10H-3, 145-150	89.05	7.47	5.82	34.0	560	22.7	474	50.1	10.5	11.4	923	382	10
11H-3, 145-150	98.55	7.50	5.79	34.0	560	22.4	478	50.1	10.7	11.2	945	413	10
15H-3, 140-150	136.50	7.38	5.96	34.0	559	21.5	474	48.4	11.8	10.8	927	561	8
18H-3, 140-150	165.00	7.42	6.30	34.0	559	19.6	478	45.5	12.3	10.4	874	679	12
21H-3, 140-150	193.50	7.35	6.77	34.0	558	17.9	479	44.0	12.8	10.1	953	701	55
24X-2, 140-150	220.40	7.39	6.04	34.0	558	19.1	472	44.1	11.8	10.5	807	603	97

Table T14. *P*-wave velocities measured at discrete intervals, Hole 1169A.

Core, section, interval (cm)	Depth (mbsf)	PWS1 (km/s)	PWS2 (km/s)	PSW3 (km/s)
189-1169A-				
1H-1, 50.00	0.50	1.582	1.576	1.856
1H-1, 50.00	2.00	1.594	1.589	1.862
1H-3, 50.00	3.50	1.551	1.543	1.802
1H-4, 89.80	5.40	1.514	1.505	1.757
1H-6, 49.90	8.00	1.518	1.509	1.746
2H-2, 49.90	10.60	1.536	1.541	1.784
2H-3, 49.90	12.10	1.551	1.553	1.810
2H-4, 50.00	13.60	1.582		1.881
3H-2, 50.00	20.10	1.608	1.570	1.887
3H-3, 50.00	21.60	1.577	1.573	1.813
3H-4, 49.90	23.10			1.810
3H-4, 50.00	23.10	1.561	1.554	
3H-5, 50.00	24.60	1.544	1.541	1.795
3H-6, 50.00	26.10	1.560	1.551	1.828
4H-1, 49.90	28.10	1.559	1.577	
4H-3, 50.00	28.25			1.798
4H-2, 50.00	29.60	1.539	1.545	
4H-4, 50.00	29.70			1.782
4H-3, 50.10	31.10	1.583	1.587	1.840
4H-4, 50.00	32.60	1.585	1.577	1.858
4H-5, 50.00	34.10	1.582	1.579	1.833
4H-6, 50.00	35.60	1.565	1.555	1.828
5H-1, 50.00	37.60	1.572	1.586	
5H-1, 50.90	37.61			1.840
5H-2, 49.10	38.63	1.550	1.542	
5H-4, 112.50	42.26	1.540		
7H-4, 48.10	61.08	1.556	1.569	1.854
7H-5, 28.90	62.39	1.552		
7H-5, 49.30	62.59		1.551	1.852
7H-6, 49.20	64.09	1.596		1.889
7H-7, 48.50	65.58	1.608	1.607	1.869
8H-2, 49.00	67.59	1.604	1.603	1.879
8H-3, 48.50	69.08	1.582	1.582	1.841
8H-4, 48.40	70.58	1.552	1.561	1.811
8H-5, 48.80	72.09	1.546	1.542	1.816
8H-6, 49.00	73.59		1.556	1.830
9H-1, 48.50	75.58	1.576	1.582	1.843
9H-2, 48.90	77.09	1.584		
9H-2, 49.50	77.10		1.588	1.871
9H-3, 51.60	78.62	1.597	1.617	1.881
9H-4, 48.50	80.08	1.557	1.553	1.819
9H-5, 41.70	81.52	1.544	1.563	1.828
9H-6, 41.10	83.01	1.544	1.567	1.827
12H-1, 47.70	104.08	1.559	1.580	1.880
21H-3, 52.30	192.62	1.624		1.968

Notes: All *P*-wave velocities measured at discrete intervals along the core. PSW1 = measured along the core, PSW2 = measured perpendicular to the core, PSW3 = measured across the core (Hamilton frame).

Table T15. Undrained shear strength from miniature vane-shear measurements, Hole 1169A.

Core, section, interval (cm)	Depth (mbsf)	Undrained shear strength (kPa)
189-1169A-		
1H-2, 100.2	2.50	20.070
1H-3, 109.9	4.10	20.957
1H-4, 125.2	5.75	18.851
1H-6, 60.4	8.10	20.070
2H-2, 99.6	11.10	21.290
2H-3, 99.2	12.59	2.440
2H-4, 86.9	13.97	21.733
3H-2, 99.2	20.59	14.304
3H-3, 98.5	22.08	24.728
3H-4, 99.0	23.59	15.080
3H-5, 99.4	25.09	20.514
3H-6, 99.2	26.59	20.403
4H-1, 114.2	28.74	26.058
4H-2, 109.5	30.19	24.506
4H-3, 99.1	31.59	14.193
4H-4, 99.1	33.09	23.175
4H-5, 99.1	34.59	13.306
4H-6, 99.0	36.09	13.195
5H-1, 60.8	37.71	32.489
5H-2, 97.2	39.11	11.865
5H-4, 140.0	42.54	25.393
7H-4, 94.8	61.55	11.754
7H-6, 95.4	64.55	25.947
7H-7, 47.8	65.58	6.653
8H-2, 94.6	68.05	21.623
8H-3, 94.7	69.55	31.713
8H-4, 94.5	71.04	11.976
8H-5, 94.4	72.54	26.723
8H-6, 77.3	73.87	24.617
9H-1, 94.7	76.05	66.088
9H-2, 92.2	77.52	50.120
9H-3, 100.0	79.10	34.042
9H-4, 97.8	80.58	34.264
9H-5, 90.8	82.01	28.498
9H-6, 83.7	83.44	30.050
12H-1, 47.5	104.07	11.865
21H-3, 53.6	192.64	23.397

Table T16. Thermal conductivity measured on whole-core sections, Hole 1169A.

Core, section, interval (cm)	Depth (mbsf)	Thermal conductivity (W/[m·K])
189-1169A-		
1H-3, 75	3.75	1.049
2H3, 75	12.35	0.923
3H-3, 75	21.85	1.001
4H-3, 75	31.35	1.082
5H-3, 75	40.39	1.138
6H-3, 75	50.35	0.923
7H-3, 75	59.85	1.099
14H-3, 75	124.85	1.134
15H-3, 75	135.85	1.013
16H-3, 75	145.35	1.13
17H-3, 75	154.85	1.129
18H-3, 75	164.35	1.261

Table T17. Index properties measured at discrete intervals, Hole 1169A.

Core, section, interval (cm)	Depth (mbsf)	Water content (bulk wt%)	Density (g/cm^3)		Porosity (%)
			Wet bulk	Dry bulk	
189-1169A-					
1H-1, 70.0-72.0	0.70	42.0	1.594	0.924	65.4
1H-2, 70.0-72.0	2.20	44.0	1.564	0.876	67.2
1H-3, 70.0-72.0	3.70	44.4	1.558	0.867	67.5
1H-4, 84.0-86.0	5.34	43.6	1.571	0.886	66.9
2H-1, 128.0-130.0	9.88	44.3	1.560	0.869	67.4
2H-3, 70.0-72.0	12.30	42.7	1.596	0.915	66.5
3H-3, 70.0-72.0	21.80	39.4	1.634	0.990	62.8
3H-4, 70.0-72.0	23.30	35.6	1.708	1.100	59.3
3H-5, 70.0-72.0	24.80	37.6	1.664	1.038	61.1
3H-6, 70.0-72.0	26.30	35.9	1.702	1.091	59.7
4H-1, 70.0-72.0	28.30	32.6	1.756	1.184	55.9
4H-3, 70.0-72.0	31.30	35.6	1.696	1.092	59.0
4H-4, 70.0-72.0	32.80	36.6	1.681	1.067	60.0
4H-5, 70.0-72.0	34.30	36.2	1.691	1.079	59.7
4H-6, 70.0-72.0	35.80	36.1	1.688	1.078	59.6
5H-4, 100.0-102.0	42.14	36.3	1.682	1.072	59.6
5H-5, 70.0-72.0	43.34	35.5	1.696	1.094	58.9
7H-4, 70.0-72.0	61.30	35.5	1.708	1.101	59.3
7H-5, 70.0-72.0	62.80	36.0	1.695	1.084	59.7
7H-6, 70.0-72.0	64.30	39.7	1.635	0.985	63.4
7H-7, 61.0-63.0	65.71	36.1	1.695	1.083	59.7
8H-2, 70.0-72.0	67.80	36.5	1.676	1.063	59.8
8H-3, 70.0-72.0	69.30	35.5	1.701	1.097	59.0
8H-4, 70.0-72.0	70.80	35.3	1.706	1.104	58.7
8H-5, 70.0-72.0	72.30	36.2	1.697	1.082	60.0
8H-6, 70.0-72.0	73.80	36.3	1.681	1.071	59.5
8H-7, 50.0-52.0	75.10	47.0	1.507	0.799	69.1
9H-1, 70.0-72.0	75.80	35.4	1.682	1.086	58.2
9H-2, 70.0-72.0	77.30	35.3	1.688	1.092	58.2
9H-3, 40.0-42.0	78.50	31.4	1.782	1.222	54.7
9H-4, 70.0-72.0	80.30	38.2	1.631	1.007	60.9
9H-5, 51.0-53.0	81.61	33.2	1.743	1.165	56.4
9H-6, 70.0-72.0	83.30	33.1	1.745	1.168	56.4
10H-1, 97.0-99.0	85.57	30.9	1.782	1.231	53.8
12H-1, 63.0-65.0	104.23	35.6	1.692	1.090	58.8
15H-2, 70.0-72.0	134.30	34.7	1.731	1.131	58.6
15H-4, 70.0-72.0	137.30	39.9	1.620	0.974	63.1
19H-1, 70.0-72.0	170.80	17.6	1.848	1.523	31.7
19H-3, 50.0-52.0	173.60	28.5	1.835	1.313	51.0
20H-3, 70.0-72.0	183.30	27.5	1.857	1.345	49.9
21H-3, 70.0-72.0	192.80	29.7	1.818	1.278	52.8
21H-6, 100.0-102.0	197.60	31.8	1.767	1.204	54.9
22X-1, 70.0-72.0	199.30	37.5	1.680	1.049	61.5
23X-2, 70.0-72.0	210.10	33.5	1.743	1.158	57.1
23X-4, 70.0-72.0	213.10	36.0	1.711	1.095	60.1
24X-1, 70.0-72.0	218.20	36.4	1.697	1.079	60.3
24X-3, 70.0-72.0	221.20	36.2	1.704	1.087	60.2
25X-1, 77.0-79.0	227.87	36.3	1.694	1.079	60.1
25X-3, 80.0-82.0	230.90	35.7	1.702	1.095	59.3
26X-1, 70.0-72.0	237.40	33.9	1.748	1.155	57.9
26X-3, 70.0-72.0	240.40	35.7	1.703	1.095	59.4
26X-5, 70.0-72.0	243.40	34.6	1.721	1.126	58.1